Journal of Structural Geology 32 (2010) 606–622

Contents lists available at ScienceDirect

Journal of Structural Geology

journal homepage: www.elsevier.com/locate/jsg

Orientation-related deformation mechanisms of naturally deformed amphibole in amphibolite mylonites from the Diancang Shan, SW Yunnan, China

Shuyun Cao [a,b,*], Junlai Liu [b], Bernd Leiss [a]

[a] Geoscience Centre, University of Göttingen, Göttingen 37077, Germany
[b] State Key Laboratory of Geological Processes and Mineral Resources (GPMR), China University of Geosciences, Beijing 100083, China

ARTICLE INFO

Article history:
Received 2 February 2009
Received in revised form
11 March 2010
Accepted 29 March 2010
Available online 3 April 2010

Keywords:
Amphibole mylonites
Micro- and sub-microstructures
Fabric analysis
Twinning nucleation recrystallization
Diancang Shan of Yunnan

ABSTRACT

Sheared amphibolite rocks from Diancang Shan high-grade metamorphic complex along the Ailao Shan-Red River shear zone, southwestern Yunnan, China, show typical mylonitic microstructures. The mylonites are characterized by porphyroclastic microstructures and the ultramylonites are highly lineated with alternating amphibole- and quartzofeldspathic domains. Microstructural analysis and P/T estimation suggest that the amphibole grains in the mylonitic rocks are deformed and dynamically recrystallized at amphibolite facies.

In the mylonitic amphibolites, there are two types of amphibole porphyroclasts, i.e. type I "hard" and type II "soft" porphyroclasts. They have their [001] crystallographic orientations subnormal and sub-parallel to the stretching lineation of the rocks, respectively. The two types of porphyroclasts show distinct deformation microstructures and sub-microstructures formed by various deformation mechanisms, which contribute in different ways to the generation of the fine-grained matrix. Shape preferred orientation analysis, misorientation analysis of the two types of porphyroclasts and new fine grains around them further prove the generation of the fine grains in matrix from the type II porphyroclasts. The type I "hard" porphyroclasts are deformed mainly by mechanical rotation, work hardening and intragranular microfracturing. In contrast, the deformation of the type II "soft" porphyroclasts is mainly attributed to crystalline plasticity, i.e. twinning, dislocation creep and dynamic recrystallization. During the deformation of the type II porphyroclasts, the (100) [001] slip system plays a dominant role during deformation and grain size reduction of amphibole. Twinning along the active (100) slip system, in combination with dislocation creep (gliding and climbing) governs the nucleation of subgrains and formation of dynamically recrystallized fine grains, a process here named *Twinning Nucleation Recrystallization*.

1. Introduction

Amphibole is one of the most important components in middle to lower crustal rocks. The deformation behavior of amphibole provides important clues to the understanding of mechanical, rheological and physical properties of the crust (e.g. Drury and Ural, 1990; Stünitz, 1993; Barruol and Kern, 1996; Berger and Stünitz, 1996; De Meer et al., 2002; Kitamura, 2006; Díaz Azpiroz et al., 2007; Tatham et al., 2008). Amphibole typically shows brittle to ductile behavior under a wide range of deformation P-T conditions, as revealed by studies on naturally and experimentally deformed amphiboles (e.g. Rooney et al., 1970, 1975; Biermann, 1981; Hacker and Christie, 1990; Berger and Stünitz, 1996; Díaz Azpiroz et al., 2007).

Early studies on deformation of amphibole have focused on slip systems and deformation twinning in experimentally and naturally deformed amphibole crystals. The main slip systems determined in amphibole are (100) [001], (010) [001] and (hk0) [001] (e.g. Rooney et al., 1970, 1975; Dollinger and Blacic, 1975; Skrotzki, 1992; Jiang and Skrotzki, 1996). Experimental studies reveal that deformation twins are commonly ($\bar{1}01$) and rarely (100) (e.g. Rooney et al., 1970, 1975; Buck, 1970; Hacker and Christie, 1990). In naturally deformed amphibole, however, (100) twinning (e.g. Dollinger and Blacic, 1975; Biermann, 1981; Biermann and Van Roermund, 1983; Kenkmann, 2000; Imon et al., 2002) predominates over ($\bar{1}01$) and other twinning systems (e.g. Morrison-Smith, 1976; Allison and La Tour, 1977; Cumbest et al., 1989; Hacker and Christie, 1990). Observations on naturally deformed amphiboles have also revealed variations of deformation mechanisms at different P-T conditions (e.g. Allison and La Tour, 1977; Nyman et al., 1992; Babai and La Tour, 1994; Leiss et al., 2002; Imon et al., 2002, 2004; Díaz

* Corresponding author at: Geoscience Centre, University of Göttingen, Göttingen 37077, Germany. Tel.: +49 551 3912624; fax: +49 551 3914624.
E-mail addresses: scao@gwdg.de (S. Cao), jliu@cugb.edu.cn (J. Liu).

0191-8141/$ – see front matter
doi:10.1016/j.jsg.2010.03.012

Azpiroz et al., 2007). It is generally accepted that amphibole is deformed by brittle processes and concomitant breakdown reactions under greenschist facies (e.g. Brodie and Rutter, 1985) or even at amphibolite facies (Lafrance and Vernon, 1993), e.g. by microfracturing (e.g. along (110) cleavage plane, Allison and La Tour, 1977; Nyman et al., 1992) or mass transfer (Brodie and Rutter, 1985; Stünitz, 1993; Shelley, 1994; Imon et al., 2002, 2004). Dominance of dislocation activity, subgrain formation and dynamic recrystallization may occur at higher temperature and pressure conditions (Biermann and Van Roermund, 1983; Cumbest et al., 1989; Skrotzki, 1992), although it is inferred that amphibole generally does not deform significantly by intracrystalline plasticity below 650–700 °C in the presence of fluid (Berger and Stünitz, 1996).

In polyphases rocks, mineral phases (e.g. plagioclase) mostly behave in different ways during deformation. It is found that at approximately 700 °C and up to 900 MPa deformation of amphibole grains in monophase layers is characterized by crystal plasticity, but in the two-phase mixtures by granular flow (Kruse and Stünitz, 1999). Therefore, the formation of deformation microstructures and variation of deformation mechanisms of the polyphase rocks may be attributed to the leading role of chemical disequilibrium. Detailed studies on amphibole deformation at low-pressure conditions suggest that dissolution-precipitation creep and cataclastic flow, rigid body rotation within a weaker plagioclase matrix, and subgrain rotation recrystallization may explain the deformation and dynamic recrystallization at different conditions (Díaz Azpiroz et al., 2007). The texture types of amphibole and plagioclase in the polyphase rocks mostly result from varying deformation modes of the different mineral phases (Leiss et al., 2002).

From the above discussions, there still exist significant disagreements on the deformation behavior of amphibole under different conditions. It appears that the high temperature deformation of amphibole is a complex process and the dominant deformation mechanisms are still unclear. The present study on amphibolite mylonites collected from Diancang Shan, SW Yunnan, China, provides new results for and constraints on the deformation and dynamic recrystallization of amphibole at amphibolite facies conditions, by applying OM (Optical Microscope), TEM (transmission electron microscope), EPMA (electron probe microanalysis) and EBSD (electron backscattered diffraction) techniques. Microstructural, submicrostructural and LPO (lattice preferred orientation) texture studies reveal that the amphibolite mylonites and ultramylonites developed from amphibolite rocks by progressive shearing. Different mineral phases in the rocks show distinct deformation characteristics. Amphibole and plagioclase grains are intensely deformed with obvious grain size reduction, but quartz grains are recrystallized dominantly by grain growth. Initial crystallographic orientations of amphibole grains from the host rocks have strong effects on the behavior of the grains during deformation. Most fine grains are generated by combined twinning and dislocation creep of parent amphibole grains with specific preferred crystallographic and shape orientations. Twinning along (100), in combination with dislocation creep (gliding and climbing) governs the nucleation of subgrains and formation of dynamically recrystallized fine amphibole grains.

2. Geological setting and structural analysis

Large scale left-lateral strike-slip shearing along the Ailao Shan-Red River shear zone in SW China plays important roles in accommodating the southeastward extrusion of the Indochina block during Indian-Eurasian collision (e.g. Zhong et al., 1990; Lacassin et al., 1993; Leloup et al., 1993, 1995; Burchfiel and Wang, 2003; Schärer et al., 1994). Over 500 km of southeastward displacement of the Indochina block relative to the Yangtze-South China block occurred along the shear zone (e.g. Leloup et al., 2001; Liu et al., 2006; Morley, 2007) (Fig. 1a).

Several blocks of middle to lower crustal metamorphic rocks are exposed along the Ailao Shan-Red River shear zone. They appear as lens-shaped bodies and are fault-bounded from non-metamorphic Paleozoic to Cenozoic rocks to the east and weakly deformed Paleozoic and Mesozoic meta-sedimentary rocks to the west. The Diancang Shan metamorphic complex is a typical such block, which is composed of three structural units, i.e. the central high strain shear zone, the western low-grade metamorphic volcanic-sedimentary sequence in the Lanping basin, and the eastern superimposed retrograde metamorphic belt (Liu et al., 2008) (Fig. 1b).

Proterozoic metamorphic rocks, including amphibolites, amphibole-plagioclase gneisses, sillimanite schists and marbles (e.g. Sha, 1998; Sha et al., 2002), and plutonic intrusions of various ages are highly mylonitized during left-lateral shearing and are widely exposed in the central high strain shear zone. High temperature (amphibolites facies) assemblages preserved in these mylonites include: almandine, staurolite, kyanite and sillimanite in schists; tremolite, diopside, olivine, calcite and dolomite in marbles; and amphibole, garnet and plagioclase in amphibolites. Mesoscopic structures for high temperature shearing prevail in the central high strain shear zone. Complex and sheath folds formed by ductile flow are frequently observed in sheared schists and granitic mylonites. A remarkable feature of the mylonites (both metamorphic and granitic-derived) is their extremely strong stretching lineation fabrics, in contrast to poorly developed mylonitic foliation, thus forming L and L $\gg$ S tectonites. When present, mylonitic foliation strikes NNW-SSE. Stretching lineation is subhorizontal or plunge gently either to the NNW or to the SSE (Fig. 1c).

Retrograde metamorphism overprinted the high temperature metamorphic belt along the eastern flank of the Diancang Shan range and is possibly related to exhumation of the Diancang Shan high-grade metamorphic complex in a later event (or metamorphic core complex, Liu et al., 2007). Early high temperature mylonites are sheared at greenschist facies in this zone, resulting in low temperature mineral assemblages and fabrics in chloritic mylonites. Mafic minerals (e.g. amphibole and biotite) are chloritized, quartz grains are deformed by crystal plasticity, and plagioclase grains deform mainly by fracturing, forming domino and similar microstructures. Some granitic plutons are sheared into L-S tectonites instead of L and L $\gg$ S tectonites. S–C fabrics are formed with S-planes defined by flattened grain aggregates of quartz and plagioclase and C-plane by chlorite grains. Striae, mostly defined by growth of fibrous chlorite grains, are widely distributed in the easternmost part of this belt. On the other hand, mylonitic foliation from the superimposed retrograde metamorphic belt has similar attitudes to those from the central high strain shear zone, striking NW-SE and dipping to the E, but the stretching lineation shows high plunge angle angles (70°–90°).

U-Pb dating of monazite and xenotime from synkinematic granite dikes in the high temperature mylonites and ^{40}Ar–^{39}Ar dating of amphibole, biotite and muscovite suggest ductile shearing along the Ailao Shan-Red River shear zone before 22–24 Ma and cooling during exhumation of the high-grade rocks between 23 Ma and 7 Ma (e.g. Schärer et al., 1994). It is generally accepted that Cenozoic strike-slip shearing along the Ailao Shan-Red River shear zone is the main process for the occurrence of structural and microstructural assemblages in high-grade metamorphic rocks. Exhumation of the high-grade metamorphic rocks is possibly due to detachment faulting along the eastern flank of the Diancang Shan in late Cenozoic (Liu et al., 2007).

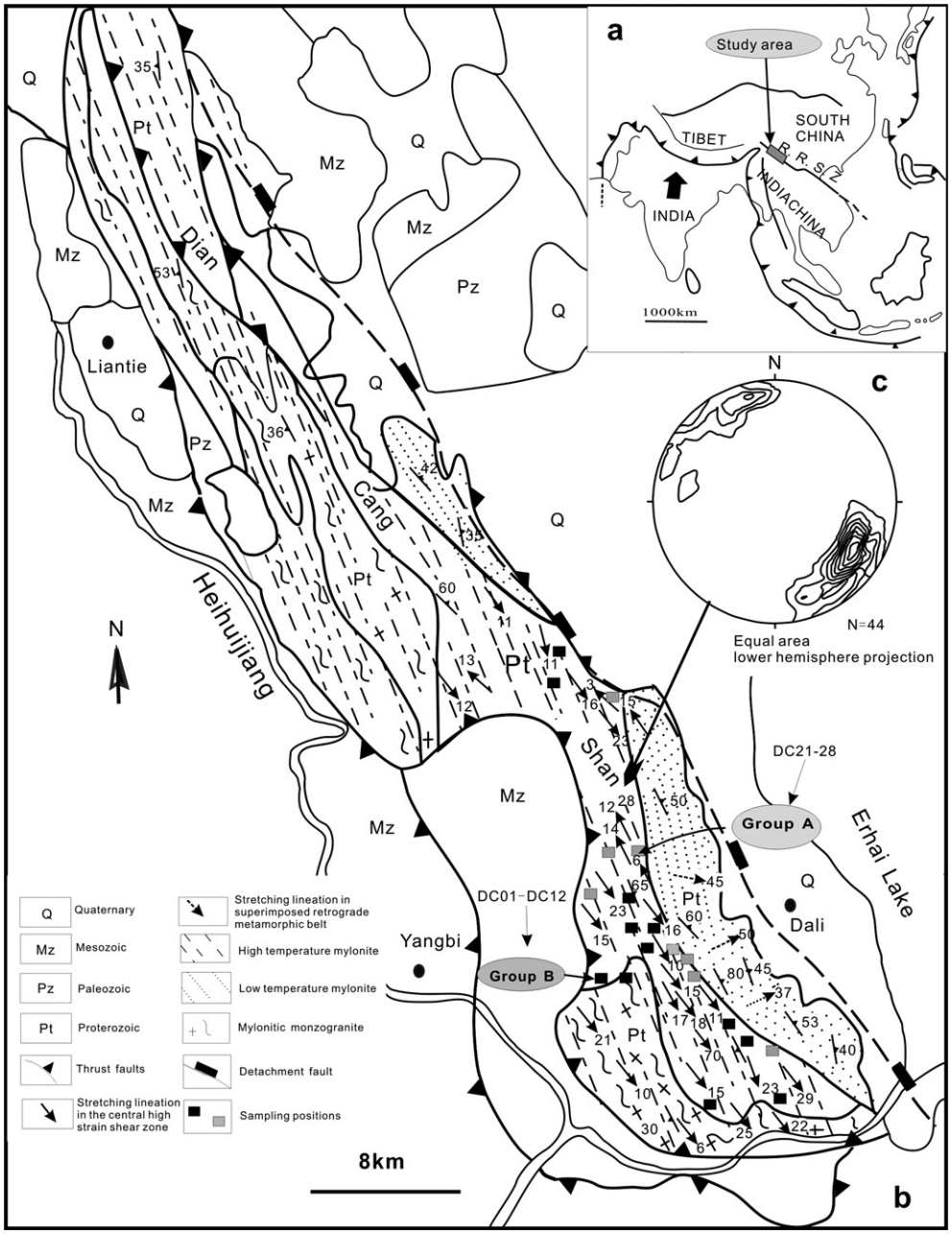

Fig. 1. Tectonic setting and structural outline of Diancang Shan area. a. regional tectonic framework of Southeast Asia. b. simplified geological map of Diancang Shan area. Group A (grey squares) comprises amphibolite mylonites and Group B (black squares) amphibolite ultramylonites. c. equal area projection of stretching lineation from high temperature mylonites. Lower hemisphere projection. R.R.S.Z = Ailao Shan-Red River Shear Zone.

3. Methods of fabric analyses

Optical microstructural observations and measurements were primarily conducted on thin sections of amphibole mylonite and ultramylonite samples. All samples were cut parallel to the kinematic XZ section, i.e. parallel to the stretching lineation and, where visible, normal to the weak foliation. Some samples were also cut parallel to the YZ section (normal to the stretching lineation and the weak foliation). XZ sections of selected samples were used to accomplish EBSD texture analyses. LPO data of amphibole were acquired with a Hitachi S-3400N-II scanning electron microscope with a tungsten filament mounted with an EBSD detector. An acceleration voltage of 20 kV applied with a beam current of 3 nA and a working distance of 20 mm resulted in 0.1 μm of spatial resolution and 0.5° of angular resolution. EBSP (electron backscatter pattern) analyses were completed using the HKL CHANNEL5 software package. LPO measurements were done using point scan and mapping modes. Point scan mode was applied to acquire EBSP data from amphibole porphyroclasts and fine grains around them in amphibole mylonites, and mapping mode with automated beam scanning was used to work on fine amphibole grains in ultramylonite.

TEM (Hitachi H-8100) observations at 20–30 kV voltages were applied to reveal the sub-microstructural features, including dislocation and twin sub-microstructures of the mylonitic rocks. EDS (Energy Dispersive Spectrometry, using an Oxford INCA Energy 350) attached on both TEM and SEM is the major technique identifying mineral phases and determining variation of mineral

components during TEM/SEM/EBSD analysis. Quantitative amphibole mineral chemistry analysis was performed by EDS on a Shimadzu EPMA-1600 electron microprobe. The probe current was 3 nA and the accelerating voltage was 15 kV. The analyses were performed on polished, carbon-coated thin sections.

4. Microstructural and submicrostructural observations

4.1. Amphibolite mylonites and two types of porphyroclasts-optical microstructures

Two groups of samples of amphibolite mylonite and ultramylonite from the central high strain shear zone in the Diancang Shan range (Figs. 1b and 2) are observed, which show different characteristics. Mylonite samples (Nos. DC21-28) (Fig. 2a) have about 15–20% relic porphyroclasts of amphiboles (Fig. 3a–e). As the most fundamental structural characteristics of the amphibolite mylonites, the strong stretching lineation and weak foliation (i.e. L or L > S fabrics) lead to alternating quartzofeldspathic and amphibole domains in sections are parallel to the L fabrics. Coarse amphibole grains mostly occur in amphibole-rich domains, while fine amphibole grains occur in quartzofeldspathic domains. Elongated coarse amphibole grains, laminated biotite grains, lens-shaped plagioclase and quartz aggregates constitute the foliation and lineation. The porphyroclasts embedded in a fine-grained matrix are the most prominent characteristics of the amphibolite mylonites, although they constitute only a minor portion of the sample volume in both the mylonites to ultramylonites. Ultramylonite samples (Nos. DC01-12) (Fig. 2b) are characterized by very few (<5%) relic amphibole porphyroclasts. Amphibole, plagioclase and biotite grains occur as extremely fine grains. Quartz forms ribbons with a thickness 160–200 μm (Fig. 3f). They are homogeneous in microstructures and grain size distribution throughout the samples.

There are two distinct types of amphibole porphyroclasts (type I "hard" and type II "soft") in the mylonitic amphibolites. They are different in their [001]-axes orientations relative to the stretching lineation:

1) Type I porphyroclasts have their crystallographic [001]-axes orientation lying in the mylonitic foliation and normal or subnormal to the stretching lineation (Fig. 3b). They are generally rounded or subrounded in shape in thin sections parallel to XZ and typically show (110) and $(1\bar{1}0)$ cleavage planes forming angles of 56°. Some grains show cleavage pairs with smaller angles suggesting [001]-axes are not always exactly perpendicular to the lineation. Type I porphyroclasts behave as "hard" porphyroclasts (e.g. Burg et al., 1986). They are fractured or have tangled dislocations (as shown in the next section), with rare evidence for intragranular plastic deformation. Such grains often have sharp boundaries and generally do not show any transition into fine grains in the matrix. Short irregular and randomly oriented intragranular fractures are only observed in some of the type I porphyroclasts. In the adjacent matrix grains, e.g. amphibole, quartz or feldspar, there is no indication of deformation related to the fracturing. Some of the fractures are cleavage fractures formed along cleavage planes, but others are not related to the crystallographic features. The former generally have long extensions or are through-going features in the entire amphibole grains. The latter are, however, generally short open cracks. They often disappear in the grains and are sometimes offset by the cleavage fractures (Fig. 3b).
2) Type II porphyroclasts have their [001]-axes orientation parallel or sub-parallel to the stretching lineation (Fig. 3c and d). They are either augen, lens or fish-shaped. A group of parallel cleavages along (110) orientation are common in the porphyroclasts. σ and φ tails are possibly formed in porphyroclasts in a stable position during general flow and δ tails are possibly around permanently rotated porphyroclasts (Passchier and Trouw, 2005; Fig. 3d). Abundant evidences for crystal plastic deformation are observed in the porphyroclasts. Undulatory or inhomogeneous extinction occurs in most of the porphyroclasts, more abundant in the cores than in the marginal zones. Microtwins are not easily detectable optically due to their micron scale in width. With ion-thinned ultrathin sections, twins are sometimes observed. They show diffuse characteristics and are thin lamellae parallel to the [001]-axes of the host grains. Their boundaries are straight and sharp. Core-mantle structures are formed due to the occurrence of subgrains with different shapes. Subgrains surrounding type II porphyroclasts are mostly equant in shape. Occasionally lamellar subgrains are in the transition between deformed cores and fine grains in the matrix. An obvious difference of the type II from the type I porphyroclasts is the gradual transition from the type II porphyroclasts into fine grains in the matrix. On both sides of the porphyroclasts, some fine grains are connected with them (Fig. 3c and d). The observation suggests that type II porphyroclasts are easily deformed by crystalline plasticity. They behave as "soft" porphyroclasts during shearing and contribute to the generation of fine grains in the matrix.

The main volume (more than 75%) of amphibolite mylonites consists of fine-grained matrix. Fine grains surrounding type I

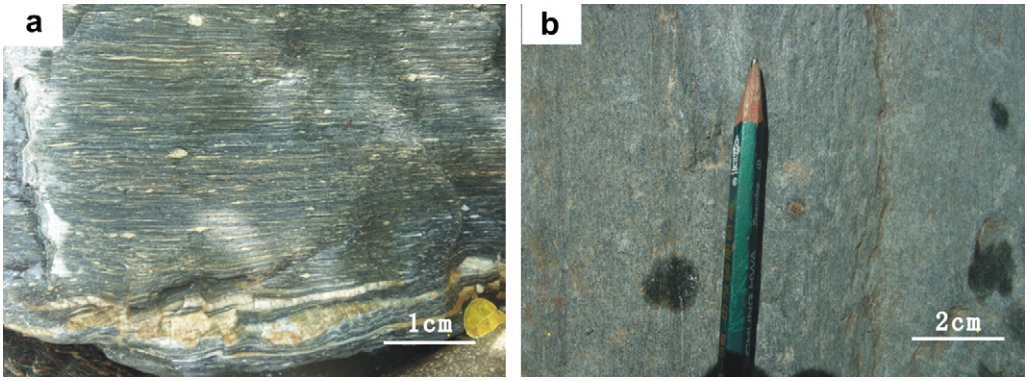

Fig. 2. Mesoscopic structures of ductile sheared amphibolites from the central high strain shear zone. a. strongly developed lineation of an amphibolite mylonite (L-fabric); b. amphibolite ultramylonite with strong stretching lineation.

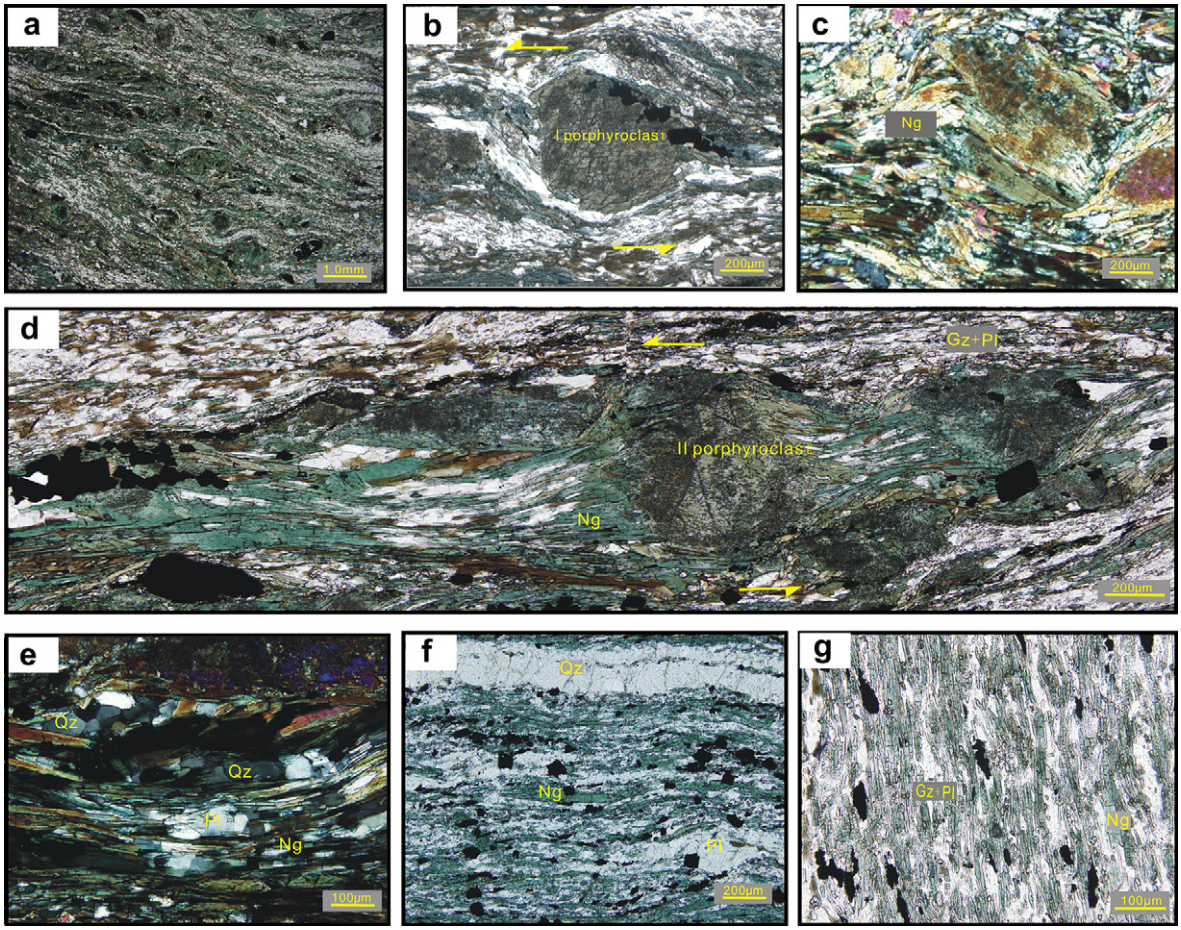

Fig. 3. Microstructures in amphibolite mylonites and ultramylonites. a. laminated and banded structures by alternating quartzofeldspathic and amphibole domains; b. type I porphyroclasts of amphibole with [001]-axes normal to the stretching lineation; c. new fine grains formed by subgrains being separated from the host grain of amphibole; d. typical type II porphyroclasts of amphibole with [001]-axes parallel to shearing direction; e. triple junctions of quartz grains, and quartz and plagioclase grains are in lens-shaped or banded distribution; f. and g. new fine grains of amphibole in ultramylonite have strong shape preferred dimensional and crystallographic orientations parallel to stretching lineation. Ng- new fine grains; QZ- quartz grains; Pl- plagioclase grains. Arrows- stretching lineation or shearing direction. a, b, c and e– cross-polarization; d, f and g- parallel polarization.

porphyroclasts are randomly oriented and do not show obvious shape and crystallographic preferred orientations. Some fine grains, however, have transitional relations with type II porphyroclast grains (e.g. fine grains are obviously distributed between φ-shaped grains, Fig. 3d). They are generally aligned in the [001]-axes direction of the porphyroclasts. Fine amphibole grains in the mylonites are characterized by the following features (Fig. 3f and g): a) they are generally single crystals; b) grains are acicular- or columnar-shaped; c) they are homogeneously distributed and have strong shape preferred orientations, forming L-fabrics of the mylonites; d) normal to the long axes of the grains there is a group of intragranular fractures; e) fine grains in the ultramylonites rarely show obvious evidences of intragranular plastic deformation, although undulatory extinction can be occasionally observed.

4.2. Optical grain size and aspect ratio analysis

The brief microfabric description about the grain sizes and shape preferred orientations (SPOs) is presented in Table 1 and Fig. 4. The long axis (A) and short axes (B) of the two types of porphyroclasts and fine grains in matrix were measured on XZ sections separately. The grain sizes $[(A + B)/2]$ and aspect ratios ($R = A/B$) are calculated using the measurements. The detailed procedure for measurement and calculation is after by Díaz Aspiroz and Fernández (2003).

The type I porphyroclasts have grain sizes ranging between 200 μm and 500 μm, while the type II porphyroclasts have a wider range of grain size variation (e.g. from 200 μm to 1.5 mm) than the type I porphyroclasts. The fine-grained amphiboles of the matrix are mostly ranging from 100 to 200 μm (Table 1). The aspect ratios of grains are closely related to the types of grains, varying from 1 to 2 for type I porphyroclasts, 2 to 5 for type II porphyroclasts and 5 to 20 for fine grains in the matrix, respectively. Two important factors may contribute to the variations in grain sizes and aspect ratios of the two types of porphyroclasts. Initial differences in their crystallographic orientations are of the first order. Mechanical rotation of the type I porphyroclasts resulted in the equant shapes in sections normal to [001]-axis. Progressive shearing of type II porphyroclasts may have contributed to the elongated grains with a large grain sizes and high aspect ratios. The small grain sizes and high aspect ratios of the fine grains in the matrix, however, are

Table 1
Grain size and aspect ratio data from mylonitic and ultramylonitic amphibolite samples.

Type	Type I porphyroclasts	Type II porphyroclasts	Fin-grained amphibole
Amphibole grain-size	200–500 μm	200μm–1.5 mm	100–200 μm
Amphibole aspect ratio	1–2	2–5	5–20

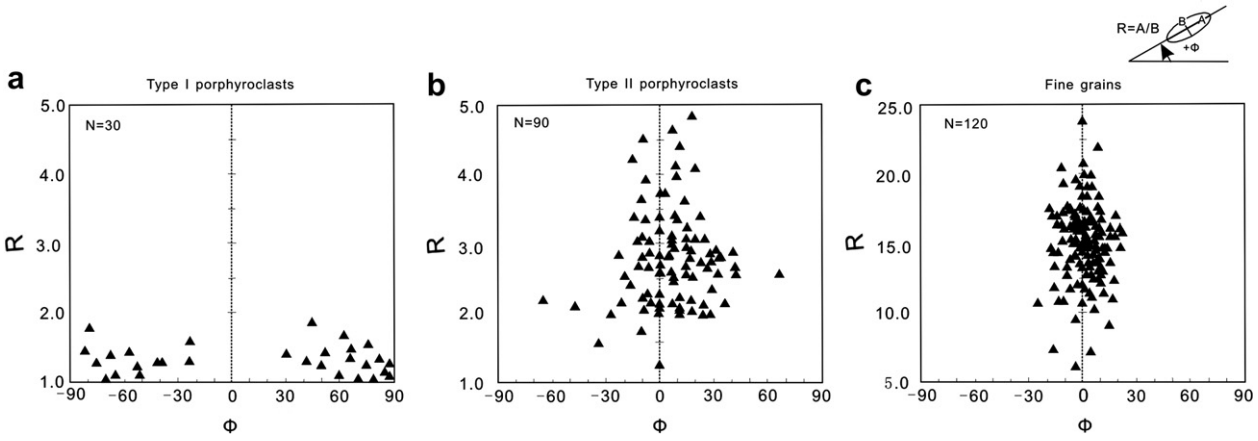

Fig. 4. ϕ- R diagram showing the relationship between the amphibole aspect ratios (R) and the orientation of long axes of the grains with respect to the foliation direction (ϕ) in the XZ section a. type I porphyroclasts; b. type II porphyroclasts; c. fine grains from matrix. (ϕ) is positive when measured anticlockwise from the foliation trace.

possibly related to the mechanisms of generation of the fine grains, as discussed in the following context.

The SPOs of amphibole grains are shown by their long axis orientations with respect to the foliation direction (ϕ), and aspect ratios (*R*). The long axis orientation of each amphibole grain was measured as the angle (ϕ, anticlockwise positive) from the foliation trace in the XZ section to the direction of the long axis (Fig. 4). In the *R*–ϕ diagram, different types of grains cluster in different ranges. The ϕ values of the type II porphyroclasts are mostly in the range from −30 to +45°, and those of the fine-grained grains cluster between −30 and +30°. They have some overlaps, but the latter are more concentrated around the $\phi = 0°$ axis. The similarity of the *R*–ϕ values of the type II porphyroclasts and fine grains in the matrix are interpreted by the deviation of the fine grains from the porphyroclasts. Their difference may be attributed to progressive rotation of the new fine grains towards a specific orientation, e.g. the direction of the kinematic lineation after separation from their parent grains. The distribution pattern of the type I porphyroclasts is, however, more randomly in the range from 30 to 90° (minus or plus). Such a random variation is possibly due to the effect of mechanical rotation, instead of plastic deformation, of the type I porphyroclasts.

4.3. Submicrostructral characterization – TEM observation

TEM analysis of the two groups of samples reveals the existence of various types of dislocation sub-microstructures in amphibole (from both deformed porphyroclasts and recrystallized grains) (Fig. 5), quartz and plagioclase grains (Fig. 6). There are free dislocations, dislocation dipoles, dislocation arrays, dislocation walls, subgrains formed by dislocation walls and twin boundaries, and tangled dislocations.

The type I porphyroclasts are hardened grains characterized by dominant tangled dislocations in the core and also in the marginal zones (Fig. 5a). They are highly entangled without obvious variation from grain to grain or within a porphyroclast. In some of the grains, different types of free dislocations are present also. Most are dipoles and few are straight free dislocations. They are probably new dislocations formed during progressive deformation. Thin deformation twins are rare and have very small lengths when occurring. Furthermore, the type I porphyroclasts generally have straight and regular grain boundaries. They are not mantled and there are no transition zones (i.e. subgrains) between the porphyroclasts and fine-grained matrix.

In type II porphyroclasts free dislocations (Fig. 5b–d) are common and are generally short lines (0.20–0.33 μm). Most of the free dislocations are not aligned to specific crystallographic orientations. Free dislocations occur in the cores of the deformed type II porphyroclasts, in the subgrains developed from the mantle of the porphyroclasts, and in some fine grains around the porphyroclasts. Those in the cores and in the subgrains are often curved, forming dislocation dipoles bulging in the direction of dislocation climb, and in most cases curving to the (001) dislocation walls (Fig. 5c). Free dislocations are self-organized into dislocation arrays (Fig. 5b) or dislocation walls (Fig. 5c), generally along (001) and (100) planes (Fig. 5c and d), implying the softened characteristic of the type II porphyroclasts. Twin boundaries often constituted by well-organized dislocations (Fig. 5c and d), suggest that they form a special type of dislocation walls. However, they differ from the other type of dislocation walls in that they are parallel arrays of dislocations that bound dislocation free domains (e.g. twins and twin hosts). Such domains are straight and narrow lamellae of micron scale in width and they are oriented parallel to specific crystallographic orientations (e.g. (100)). A very few subgrains formed by dislocation walls in different orientations, resulting in irregular or polygonal shapes. Most subgrains, however, are configured by combinations of dislocation walls and twin boundaries (Fig. 5c and d), and generally show acicular to columnar shapes (Fig. 3f and g). They are the dominant type of subgrains, possibly due to the ease of twinning at the prevailing conditions.

Fine amphibole grains in the matrix of the mylonitic rocks are extremely elongated and characterized by high aspect ratios, as also shown by the optical measurements. The grains contain very few free dislocations (Fig. 5f), probably resulting from strain accumulation during progressive deformation. Most fine grains have straight grain boundaries parallel to crystallographic [001]-axes orientation of the amphibole crystal. They are acicular or columnar shapes defined by and parallel to the configuration of twins.

The dislocation density calculation reveals great variations for the different types of grains. A significant decrease in the density is detected from the "hard-worked" type I porphyroclasts, to "softened" type II porphyroclasts and to dynamically recrystallized new fine grains, e.g. the dislocation densities are approximately 3×10^8 cm^{-2} in the type I porphyroclasts, about 5×10^8 cm^{-2} in the mantle of type II porphyroclasts, and about 2×10^3 cm^{-2} in the fine-grained amphibole grains in the matrix. Although the small size of the regions for dislocation calculation is associated with the heterogeneity of the dislocation distribution in plastically deformed materials, and may lead to the ρ-values that are not

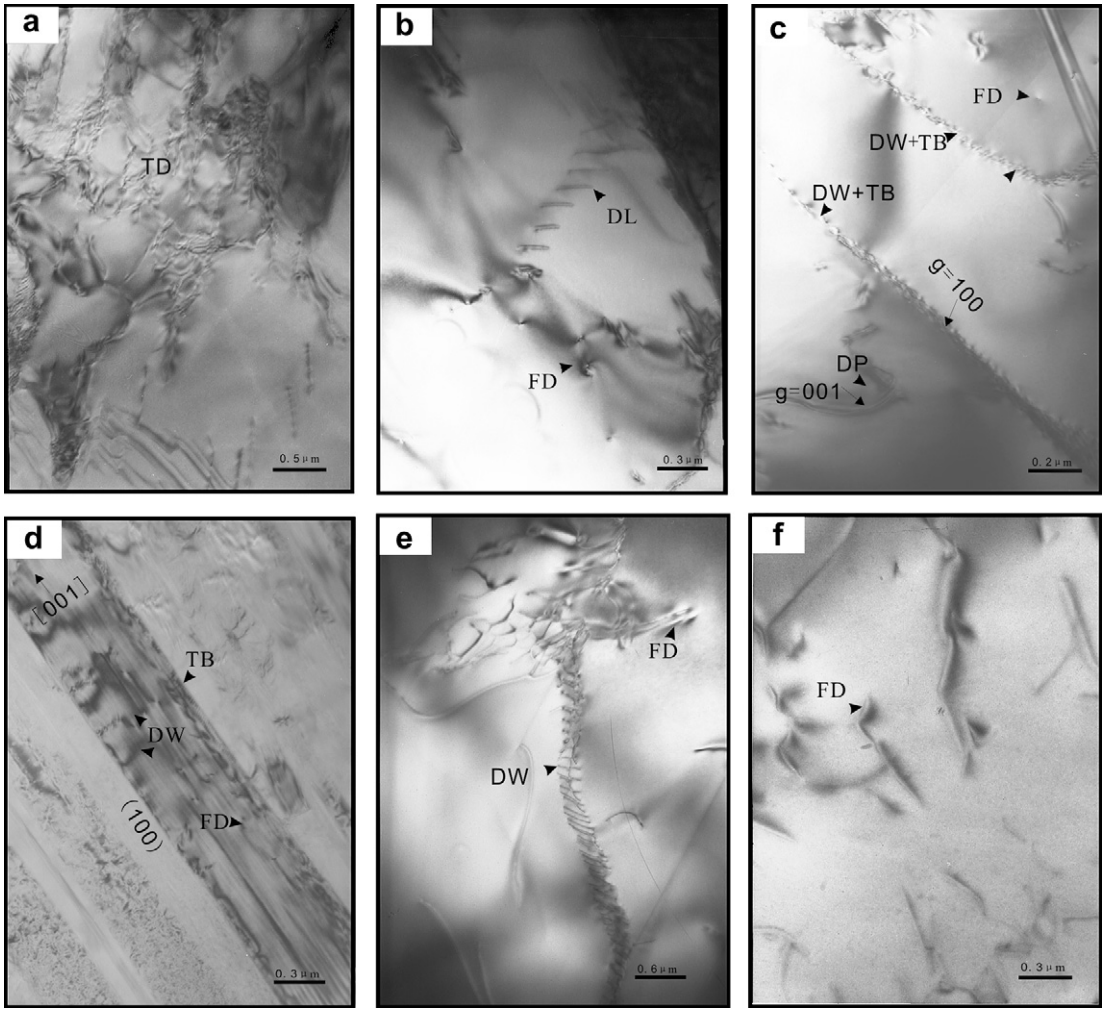

Fig. 5. Sub-microstructures of amphibole grains from mylonitic rocks. a. tangled dislocations from the core of a type I amphibole porphyroclast; b. free dislocations and regular dislocation arrays; c. dislocation dipoles, dislocation walls and free dislocations; d. regular twin boundaries, dislocations in twins and twinned hosts, and dislocation walls perpendicular to twin boundaries; e. a dislocation wall; f. fine amphibole grains containing a few free dislocations; b-e taken from margins of type II amphibole porphyroclasts; FD- free dislocation; DL- dislocation array; DP- dislocation dipole; TD- tangled dislocation; DW- dislocation wall. TB- twin boundary.

representative, or are inconsistent with the plastic behaviors of the materials, the general tendency of dislocation density variation in the different types of grains is in good correlation with the optical microscopy and TEM observations.

5. Textures -*EBSD* analysis

5.1. LPO data

Fig. 7 give some of the typical EBSD pole figures of type I porphyroclasts, fine matrix grains around the type I porphyroclasts, type II porphyroclasts, fine grains around type II porphyroclasts and fine grains from the matrix in ultramylonites. Fig. 7a gives 39 measured orientations of typical type I porphyroclast. The porphyroclast is oriented with [001]-axes parallel to *Y*. The (100)- plane is parallel to XY and normal to *Z* of the sample. In Fig. 7b the orientation pattern of fine grains around the above type I porphyroclast reveals the diversity of (100), (010) and [001]-directions of these grains. They have relatively random misorientations from the porphyroclast varying from low angles to about 90°. Such orientation patterns imply that there is no progressive transition from the type I "hard" porphyroclasts to fine grains around them and the orientation of the fine grains may have been disturbed due to the rotation of the porphyroclast.

[001]-axes and (100)-planes of the type II porphyroclasts dominantly form maxima lying in the *X* and XY orientations, respectively (Fig. 7c). Fine grains around the type II porphyroclasts have slight variations in their LPOs (Fig. 7d). Some of the secondary [001] and (100) maxima have angles up to 26° from those of the porphyroclasts, possibly reflect misorientation at the σ-, δ- or φ-shaped tails of these porphyroclasts. The majority, however, are overlapping and are transiting into the orientations of the porphyroclasts, suggesting that most of the fine matrix grains take the orientations of the orientations of their precursor type II porphyroclasts. Similar patterns exist for many of the type II porphyroclasts. The similarity of LPO patterns of the type II porphyroclasts with the fine grains around them (Fig. 7c, and d) imply that most of the new fine grains surrounding type II porphyroclasts are derived from the type II porphyroclasts and they finally become stabilized in the direction of the stretching lineation (or the shearing direction).

Mapping of fine matrix amphibole grains from samples of mylonitic and ultramylonitic amphibolites give similar LPO patterns to those of the type II porphyroclasts and fine grains around them (Fig. 7c–e). The orientation patterns are simple and are characterized by strong maxima of [001]-axis in the *X* direction and of (100) in the *Z* direction of the samples. Correspondingly (010) forms a maximum in the *Y* direction. Such similarity in LPO patterns of the different types of grains provides further

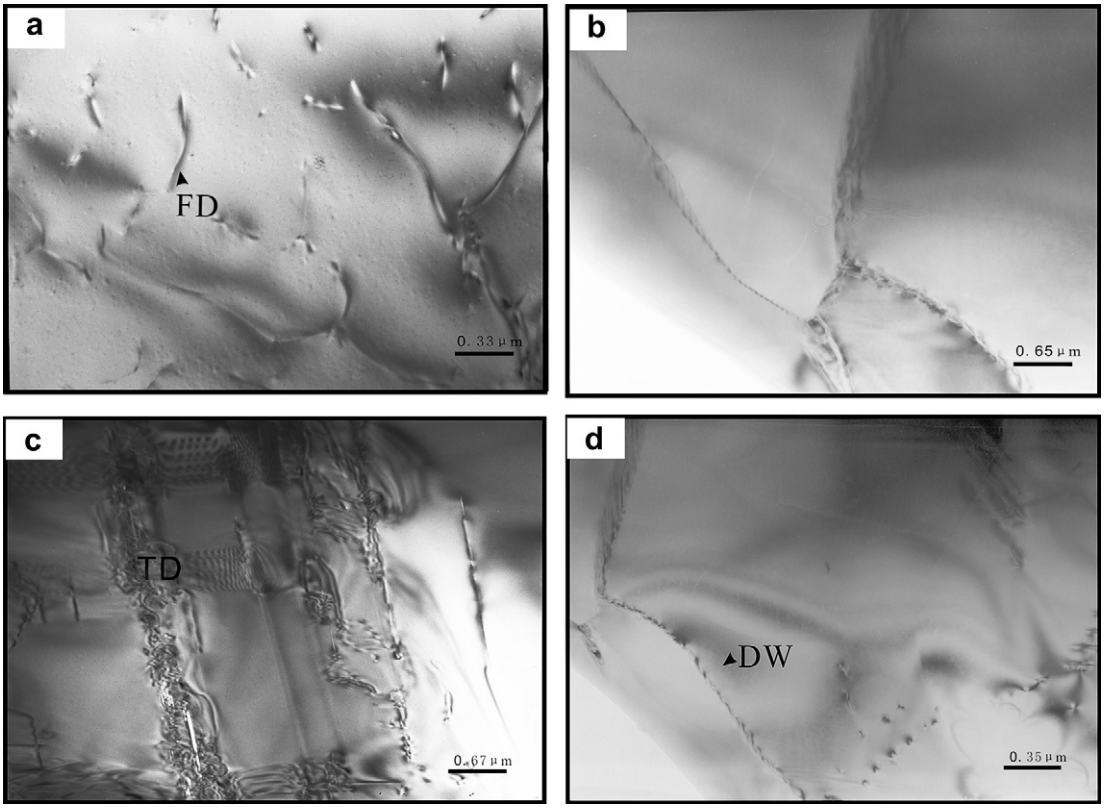

Fig. 6. Deformation sub-microstructures in quartz and plagioclase grains from amphibolite mylonitic rocks. a. very few free dislocations in quartz; b. dislocation networks or subgrains in a deformed quartz grain; c. tangled dislocations in the core of a porphyroclastic plagioclase; d. dislocation walls and a few free dislocations in deformed plagioclase grains. FD- free dislocation; TD- tangled dislocation; DW- dislocation wall.

information for the origin of matrix grains from the "soft" oriented porphyroclasts. There is a slight dispersion of (100) and (010) of matrix grains towards a girdle parallel to the YZ-plane. Such a complication of the orientation patterns is possibly due to perturbation of grain orientations by foliation inflexion or owing to perturbation by any type of porphyroclasts. It may also suggest that (1) there is a minor slight rotation of some fine grains around their [001]-axes once they become independent from their parental porphyroclasts or (2) the fine grains are formed from a secondary population of parental porphyroclasts oriented also with their [001]-axes parallel to *X* but with a different (100) and (010) orientation, considering the well documented slip system ((010) as the slip plane) in naturally and experimentally deformed amphiboles (Díaz Azpiroz et al., 2007, and references therein on page 641).

5.2. Misorientation

The crystallographic misorientation between two crystals can be described by the misorientation angle distribution (MAD) or by rotation axis (e.g. Randle, 1993; Lloyd et al., 1997; Fliervoet et al., 1999; Lapworth et al. 2002). Our misorientation analyses are based on the measurements of crystallographic orientations by the EBSD. Because the data acquisition of porphyroclasts and the fine grains around porphyroclasts was by point scan mode, these data allow us to have uncorrelated misorientation calculating their associated misorientation from the randomly selected grain pairs that are not necessarily in physical contact (Fliervoet et al., 1999). This approach is similar to the method of factorial misorientation analysis described by Lloyd et al. (1997).

The misorientations of fine grains around type I and II porphyroclasts, and fine grain matrix show obvious differences. In the uncorrelated MAD of a type I porphyroclast and fine grains around it (Fig. 8b), there is a major peak at 5–15° in coincidence with the data from the porphyroclast (Fig. 8a). The fine grains around the type I porphyroclast, however, show random distribution of misorientation angles, from 15 to 170°, implying that they do not have close relationship in view of crystallographic orientation (Fig. 8b). The MADs of the type II porphyroclasts are different from those of type I porphyroclasts. Three peaks of 0–10°, 25–65° and 105–165° misorientation angles may represent parent grains in different orientations (Fig. 8c). The MADs of fine grains around the type II porphyroclasts and in the matrix of ultramylonites, however, have obvious similarities (Fig. 8d and e). Missing low angle misorientations are different from the MADs of both the type I and type II porphyroclasts. However, they show some overlaps with those of the type II porphyroclasts. The differences and similarities of MADs of different types of grains support the idea that the matrix grains are genetically related to the fine grains around the type II porphyroclasts, and therefore to the porphyroclasts. In contrast, the type I porphyroclasts are not related to any of the other types of grains. In general, dislocation creep processes and subgrain rotation forming a strong LPO may be expected to result in a greater proportion of lower angle misorientations between grains, which may be reflected by a large peak of very low angle misorientations also on the neighbor-pair distribution (e.g. Trimby et al., 1998). The recrystallized amphiboles, however, mostly show high angles of misorientation. This may support their origin mostly from a more complicated, subgrain rotation unrelated process. Therefore, the mixed process of twinning and dislocation creep during the generation of the fine grains may have disrupted the original grain orientation relations as produced from subgrain rotation.

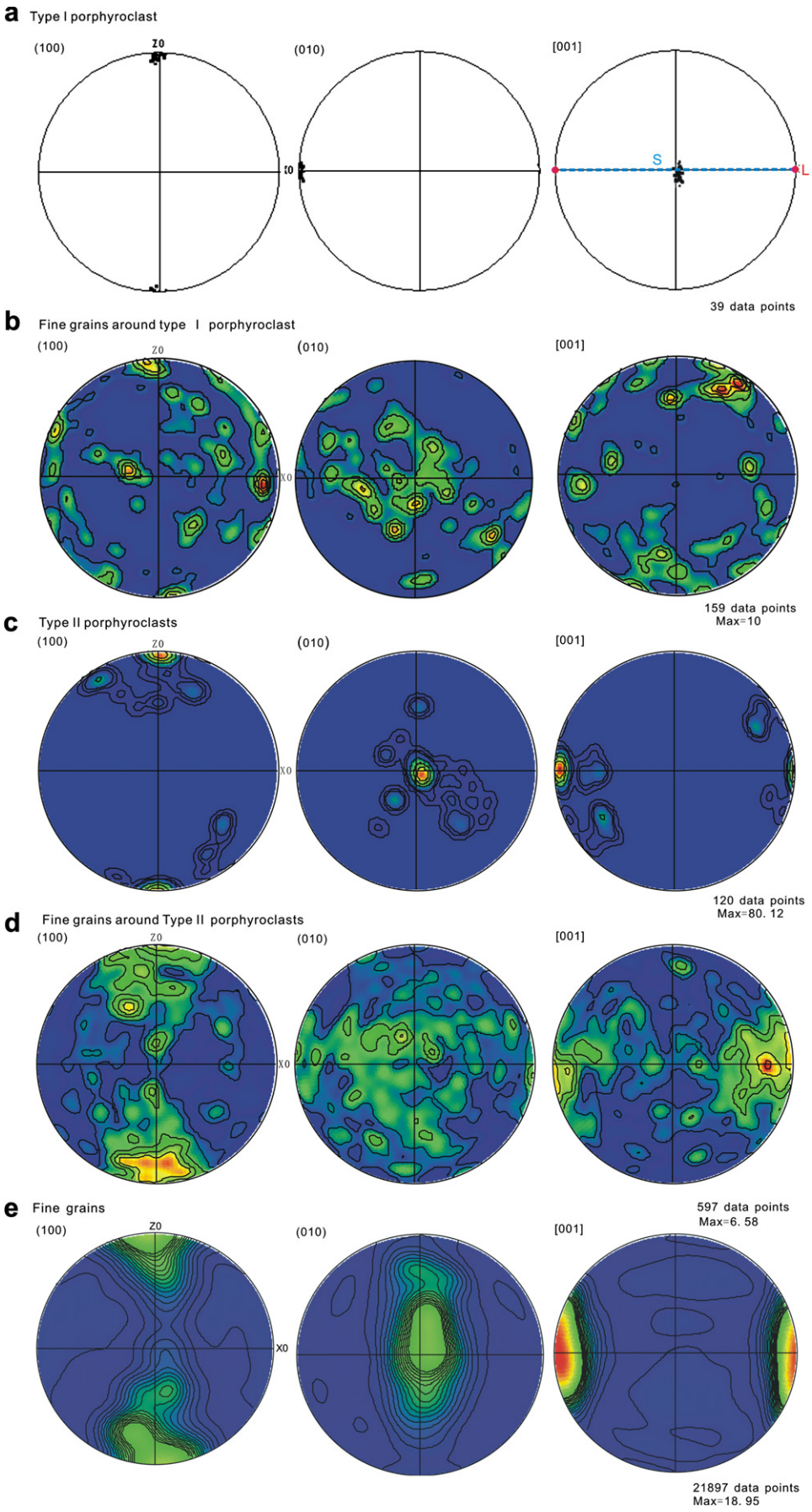

Fig. 7. EBSD fabric data of amphiboles from the mylonitic and ultramylonitic amphibolites. a. orientation of a type I porphyroclast; b. fabrics of a type I porphyroclast and fine grains around it. c. fabrics of type II porphyroclasts. d. fabrics of fine grains around the type II porphyroclasts; e. fabrics of fine grains from matrix of ultramylonites. Foliation is XY- broken line and lineation is *X* direction in this plane. Equal area and lower hemisphere projection, couture lines are multiples of random distribution.

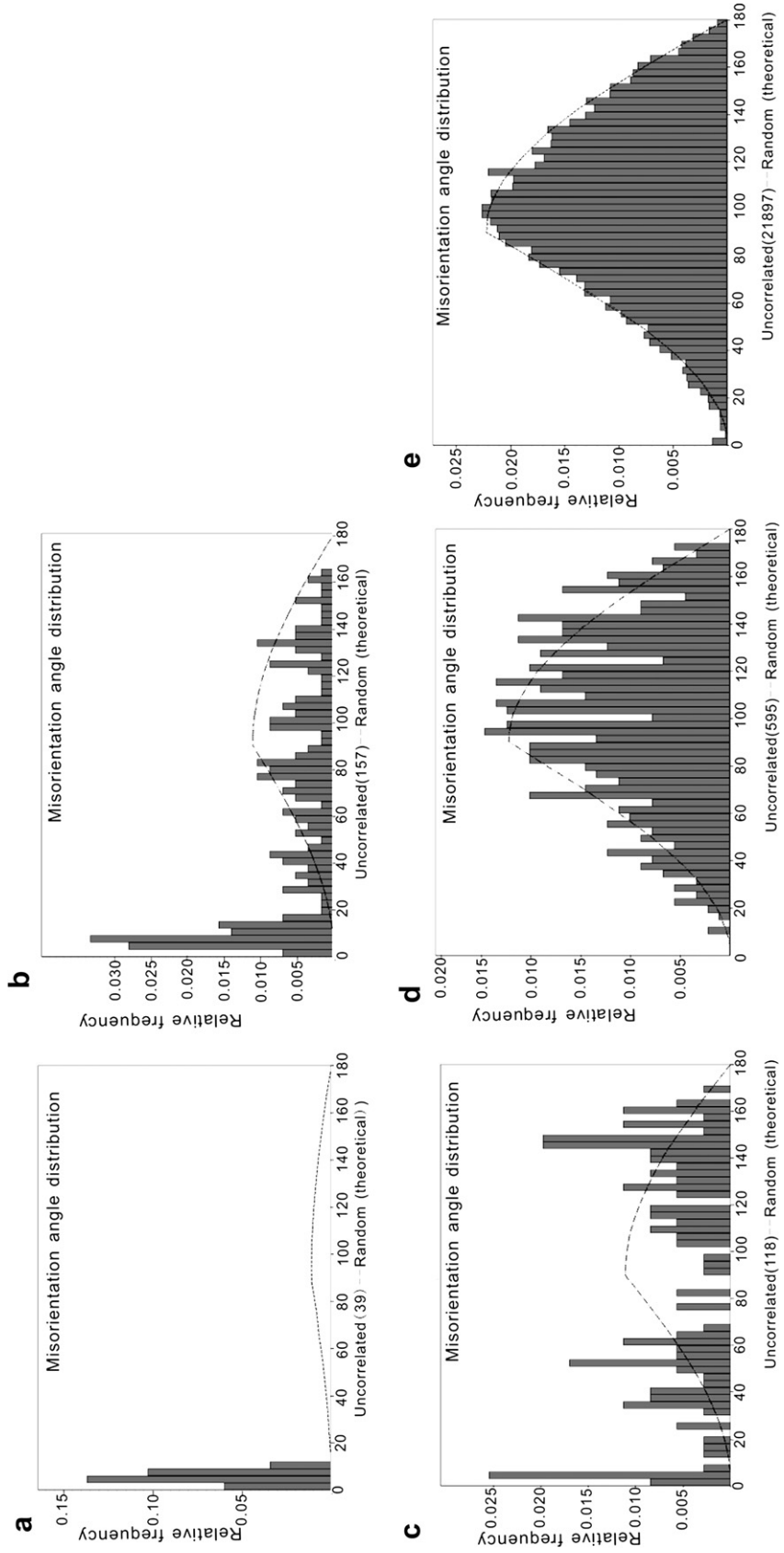

Fig. 8. Misorientation angle frequency distributions of amphiboles. a. type I porphyroclasts; b. fine grains around type I porphyroclasts and type I porphyroclasts; c. type II porphyroclasts; d. fine grains around type II porphyroclasts; e. fine grains in the matrix. The theoretical random distribution curve for amphibole is shown for comparative purposes.

Inverse pole figures for both type I and type II porphyroclasts and their surrounding matrix (Fig. 9) provide further information on differences in the misorientation of the fine grains from the porphyroclasts. Data points from a type I porphyroclast show strong clustering of *X*0//[010], *Y*0//[100] and *Z*0//[001], but fine grains around them show scattered distributions (Fig. 9a). Type II porphyroclasts and fine grains around them, however, have similar distribution patterns in the inverse pole figure (Fig. 9b), X0//[001], Y0//[010] and Z0//[100].

The inverse pole figure analyses provide clues to the close relationships between the fine grains and the type II porphyroclasts. The distribution pattern of data points of fine grains around the type II porphyroclasts is interpreted as derivation of the fine grains from the porphyroclasts. To the contrary, they also suggest that the orientation of the fine grains are not related to the type I porphyroclasts.

6. Mineral chemistry analysis of amphibole-plagioclase and P-T estimation

Metamorphic mineral assemblages, and deformation structures or microstructures suggest that the mylonitic amphibolites are primarily deformed under the amphibolite facies conditions. In metamafic rocks in which plagioclase and amphibole are in fabric equilibrium, amphibole mineral chemistry and thermobarometry (Table 2) provide the opportunity to constrain the P-T conditions of deformation. A first pressure estimation is based on the metamorphic mineral assemblages of garnet+plagioclase-muscovite-biotite in staurolite-grade pelitic schists outcropping near the mylonitic amphibolites, that gives lower to medium-pressure (e.g. about 5.0 kbar) metamorphic conditions during left-lateral shearing (Leloup et al., 1993).

Electron microprobe analyses (Table 2) reveal a very slight variation in chemical compositions for the amphibole from the different types of grains (type I and II porphyroclasts, and fine matrix grains). In the amphiboles the cation distribution of Na in M4-site ranges from 0.07 to 0.23 < 0.5, in A-site between 0.20 and 0.49, and the $(Ca + Na)^{M4}$ is above 1.5 for all the samples. Therefore, it is concluded that all amphibole grains analyzed are of calcium-amphibole composition. Si and A-site occupancy are important in evaluating the composition variation of amphiboles in the mylonitic amphibolites (e.g. Pe-Piper, 1988; Díaz Azpiroz et al., 2007). Si is 6.42–6.78 p.f.u. and $(Na + K)^{A}$ ranges between 0.31and 0.63. As shown in Table 2 and Fig. 10, in the Si–Mg# diagram ($(Na + K)^{A} < 0.5$), JLDC7 and JLDC3 are plotted as magnesiohornblende and JLDC6 as tschermakite (Fig. 10a), and in the Al–Mg# diagram ($(Na + K)^{A} > 0.5$), JLDC1, JLDC2, JLDC5, belong to edenite, and JLDC4 and DC0502 are plotted close to the edenite and ferrohornblende boundary. DC0503 is plotted in the area of the pargasite (Fig. 10b). Both the Si–Mg# diagram and Al–Mg# diagram are in coincidence with Si–$(Na + K)^{A}$ # diagram (Fig. 10c). Thus the porphyroclasts and matrix grains can be grouped as edenite.

The Al^{iv}, Fe^{3+} and Ti in the octahedral sites, together with the A-site occupancy are balanced by Al^{vi} substituting (e.g., Spear, 1981; Blundy and Holland, 1990). Qualitative temperature estimations can be therefore presented on the basis of Al^{iv}, Ti and $(Na + K)^{A}$ contents in amphiboles (e.g. Spear, 1981, 1993; Blundy and Holland, 1990; Díaz Azpiroz et al., 2007). For all samples, Ti contents are low (0.01–0.06) and do not show obvious variation from porphyroclasts to matrix. The amphibole grains are characterized by high Al (Al^{iv} = 1.22–1.58, Al^{vi} = 0.43–0.73). Such characteristics may suggest that they are deformed at relatively high grades (e.g. epidote amphibolite facies to amphibolite facies, Robison et al., 1971; Spear, 1981; Anderson and Smith, 1995; Ernst and Liu, 1998). On the other hand, all the samples fall into a limited area on the $Al^{iv} - Al^{vi} + Fe^{3+} + Ti + (Na + K)^{A}$ plot (Fig. 10d), suggesting that the amphiboles meet the ideal substitution mechanism (e.g. Díaz Azpiroz et al., 2007). According to the calibration by Brown (1997), pressures of less than 6 kbar are estimated from the Na^{M4}–Al^{vi} plot for the studied amphiboles (Fig. 10e).

More precise estimation of temperature conditions of amphibolite deformation processes are further performed by applying Holland and Blundy (1994) amphibole-plagioclase geothermometer based on the edenite + albite = richterite + anorthite equilibrium. The cores of Type I and Type II porphyroclasts, and the fine grains around the porphyroclasts and in the matrix give temperatures ranging from 585 to 673 °C, with an average of 625 °C. The calculated results (Table 2) are consistent with the mineral chemistry analysis, suggesting metamorphic conditions at lower amphibolite facies at relatively lower pressures conditions.

7. Discussion

7.1. "Soft" – "hard" behavior of amphibole porphyroclasts

Amphibole grains with "hard" or "soft" initial crystallographic orientations have strong effects on the rheological behavior of the minerals. Therefore, the two types of porphyroclasts (type I and II porphyroclasts) tend to be deformed in a brittle manner at the very beginning of shearing under the prevailing conditions. The "soft" and "hard" behavior of a porphyroclast is proven by microstructural, SPO and LPO, and TEM submicrostructural analyses. Such behavior of the porphyroclast is mainly dependent on its initial crystallographic orientation with respect to applied shear stresses. When a grain is oriented with its slip system (100) [001] consistent with regional shearing, with an angle of 0°–50° or 150°–180° of the (100)- plane to the shearing direction, the slip system can be easily activated. However, when its slip system (100) [001] is inconsistent with regional shearing, with an angle of 50°–150° of the (100)-plane to shearing direction, the slip system remains unactivated (e.g. Liu, 1999). The geometrical consistency or inconsistency of the (100) [001] slip system in respect to the applied shear stresses, leads to the "soft" or "hard" behavior of the porphyroclasts during shearing.

Type I porphyroclasts are typical "hard" porphyroclasts during shearing without any evidences for dynamic recrystallization. Mechanical rotation is responsible for the deformation and orientation pattern of the type I porphyroclasts. Matrix grains around them do not have any genetic, i.e. geometrical relationships with them and behave passively during shearing, shown by SPO and EBSD analyses. Therefore, tangled dislocations or walls of tangled dislocations are preserved either at grain margins, or in the cores. There are no regular dislocation walls, implying the incapability for dislocations to glide and climb. Type II porphyroclasts are typical "soft" porphyroclasts and have mantled microstructures. Tangled dislocations are partly developed in the cores of the porphyroclasts. Along the margins of the porphyroclasts, however, dislocations are generally well organized, that some dislocation glide or climb along the (100) [001] slip system towards the (001) direction to form (001) dislocation walls. (100) micro-twinning extensively develops contemporaneously. Dynamic recrystallization by combined subgrain nucleation due to twinning and dislocation creep generates fine grains of amphibole in the matrix.

Differences in initial crystallographic orientations contribute to the "hard" and "soft" behaviors of the amphibole grains, characterized by the dislocation (im)mobility during deformation, revealed by TEM microstructural evidences. The different behaviors, on the other hand, have resulted in the similarities and

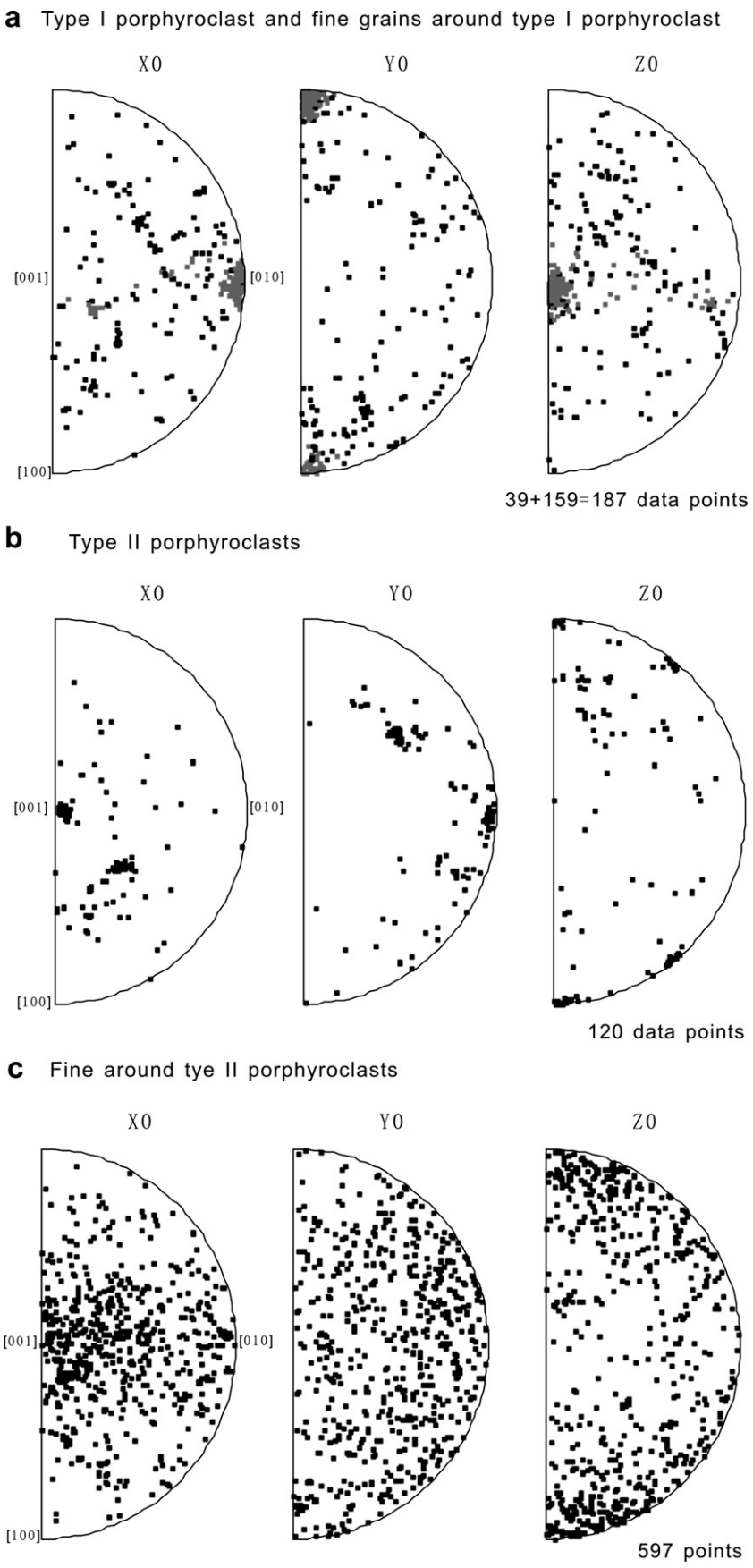

Fig. 9. EBSD inverse pole figure in the crystallographic reference frame [100], [010] and [001]. a. a type I porphyroclast and fine grains around it (the light color is from the type I porphyroclast); b. type II porphyroclasts; c. fine grains around type II porphyroclasts.

Table 2
Mineral chemistry analyses of amphibole and P-T estimation/calculation. Fe^{3+} estimated using Holland and Blundy (1994); Temperatures calculated from Hb-Pl thermometer (Holland and Blundy, 1994) at a 6 kbar present highest temperatures registered by each sample. Names according to Leake et al. (1997) and Pe-Piper (1988).

Sample	JLDC1	JLDC2	JLDC3	JLDC4	JLDC5	JLDC6	DC0501	DC0502	DC0503
Amphibole	Type I porphyroclasts		Type II porphyroclasts		Fine-grained amphibole		Ultramylonites amphibole		
SiO_2	44.13	44.35	44.54	43.25	43.07	43.10	45.60	43.13	42.51
Al_2O_3	10.70	10.81	11.62	11.53	11.34	12.15	9.67	12.70	11.26
TiO_2	0.35	0.47	0.26	0.47	0.27	0.17	0.46	0.56	0.51
Cr_2O_3	0.00	0.43	0.00	0.00	0.00	0.00	0.00	0.00	0.00
FeO	18.12	17.74	19.10	18.16	19.07	19.48	18.57	18.08	18.96
MnO	0.14	0.52	0.45	0.23	0.23	0.43	0.00	0.19	0.54
MgO	9.70	9.60	8.59	8.76	9.35	8.84	9.77	8.89	9.08
CaO	11.77	11.73	10.71	12.16	11.70	11.54	11.82	12.16	11.75
Na_2O	1.82	2.22	1.50	2.00	2.10	1.62	1.40	1.85	1.91
K_2O	0.48	0.29	0.55	0.60	0.30	0.42	0.46	0.31	0.67
Total	**97.21**	**98.16**	**97.32**	**97.16**	**97.43**	**97.75**	**97.77**	**97.87**	**97.19**
Structural formulae in base of 23 oxigens									
Si	6.61	6.62	6.64	6.54	6.46	6.42	6.78	6.48	6.42
Al^{iv}	1.39	1.38	1.36	1.46	1.54	1.58	1.22	1.52	1.58
T	**8.00**	**8.00**	**8.00**	**8.00**	**8.00**	**8.00**	**8.00**	**8.00**	**8.00**
Al^{vi}	0.50	0.52	0.68	0.60	0.46	0.56	0.48	0.73	0.43
$Al_{(total)}$	1.89	1.90	2.04	2.06	2.00	2.14	1.70	2.25	2.01
Ti	0.04	0.05	0.03	0.05	0.03	0.02	0.05	0.06	0.06
Cr	0.00	0.00	0.00	0.00	0.00	0.00	0.00	0.00	0.00
Fe^{3+}	0.41	0.32	0.55	0.20	0.57	0.71	0.38	0.36	0.56
Mg	2.19	2.14	1.91	1.98	2.09	1.96	2.17	1.97	2.04
Fe^{2+}	1.86	1.90	1.78	2.10	1.80	1.70	1.93	1.89	1.84
Mn	0.02	0.07	0.06	0.03	0.03	0.05	0.000	0.02	0.07
M1-3	**5.00**	**5.00**	**5.00**	**5.00**	**5.00**	**5.00**	**5.00**	**5.00**	**5.00**
Mg	0.00	0.00	0.00	0.00	0.00	0.00	0.00	0.00	0.00
Fe^{2+}	0.00	0.00	0.06	0.00	0.02	0.00	0.00	0.00	0.00
Mn	0.00	0.00	0.00	0.00	0.00	0.00	0.00	0.00	0.00
Ca	1.91	1.88	1.71	1.97	1.88	1.84	1.88	1.92	1.89
Na	0.11	0.12	0.23	0.07	0.12	0.14	0.12	0.09	0.11
M4	**2.00**	**2.00**	**2.00**	**2.00**	**2.00**	**2.00**	**2.00**	**2.00**	**2.00**
Ca	0.00	0.00	0.00	0.00	0.00	0.00	0.00	0.00	0.00
Na	0.42	0.49	0.20	0.51	0.49	0.33	0.29	0.45	0.45
K	0.09	0.06	0.11	0.12	0.06	0.08	0.09	0.06	0.13
A	**0.51**	**0.54**	**0.31**	**0.63**	**0.55**	**0.41**	**0.38**	**0.51**	**0.58**
Ca^{M4}	1.888	1.867	1.711	1.926	1.880	1.842	1.883	1.915	1.894
Si (p.fu.)	6.61	6.62	6.64	6.543	6.46	6.42	6.78	6.48	6.42
Mg#	0.52	0.53	0.51	0.49	0.54	0.54	0.52	0.51	0.53
$(Na + k)^A$	0.51	0.54	0.31	0.63	0.55	0.41	0.38	0.51	0.58
Name			Mag-Hb	Fer-Hb		Schermakite	Mag-Hb		
Plagioclase Samples									
Plagioclase									
SiO_2	59.40	61.05	64.51	61.38	61.30	63.82	61.48	61.71	61.92
Al_2O_3	23.12	23.37	19.07	22.40	23.06	22.59	23.08	23.13	22.59
TiO_2	0.23	0.00	0.00	0.00	0.00	0.03	0.00	0.21	0.45
FeO	0.01	0.28	0.00	0.00	1.08	0.00	0.00	0.66	0.70
MnO	0.00	0.11	0.00	0.00	0.17	0.00	0.00	0.00	0.00
CaO	5.89	5.13	4.28	4.83	4.54	3.24	4.96	4.22	4.05
Na_2O	10.52	9.82	12.62	10.86	8.79	10.58	9.58	10.11	10.93
K_2O	0.00	0.21	0.12	0.15	0.23	0.25	0.09	0.02	0.13
Total	**99.17**	**99.97**	**100.60**	**99.62**	**99.17**	**100.07**	**99.19**	**100.08**	**100.76**
Ca	0.29	0.25	0.20	0.23	0.23	0.15	0.24	0.20	0.19
Na	0.92	0.85	1.04	0.95	0.77	0.90	0.83	0.87	0.94
K	0.00	0.01	0.01	0.01	0.01	0.01	0.01	0.00	0.01
X_{ab}	0.76	0.77	0.84	0.80	0.77	0.84	0.77	0.81	0.82
X_{an}	0.24	0.22	0.16	0.20	0.22	0.14	0.22	0.19	0.17
P = 6 kbar	**641.1**	**650.1**	**584.6**	**597.7**	**672.7**	**613.7**	**617.4**	**595.9**	**652.3**
Temp. (°C)±20									

differences in deformation microstructures, SPO and LPO fabrics. The type I porphyroclasts are rounded and subrounded, with a low aspect ratio and a more random ϕ distribution. They have also unique LPO fabrics and misorientation patterns. The other types of grains, however, show general similarities, either in the SPO and LPO fabrics, or in misorientation patterns. Such similarities are attributed to the generation of the new fine grains in the matrix (either surrounding type I or type II porphyroclasts in mylonites, or in the matrix in ultramylonites) by crystal plastic deformation of the parent grains (e.g. the present type II porphyroclasts).

7.2. Twinning, subgrain nucleation and dynamic recrystallization

Lattice preferred orientations of minerals in a deformed rock are directly related to prevailing slip systems during deformation (e.g. Shelley, 1994; Fliervoet et al., 1999; Lee et al., 2002; Brenker et al., 2002; Díaz Azpiroz et al., 2007). It is generally accepted that during deformation a predominantly activated slip system tends to coincide with the flow direction and the flow plane, respectively (e.g. Mainprice and Nicolas, 1989). In this case, the parallelism of [001] crystallographic axes and (100) crystallographic planes of

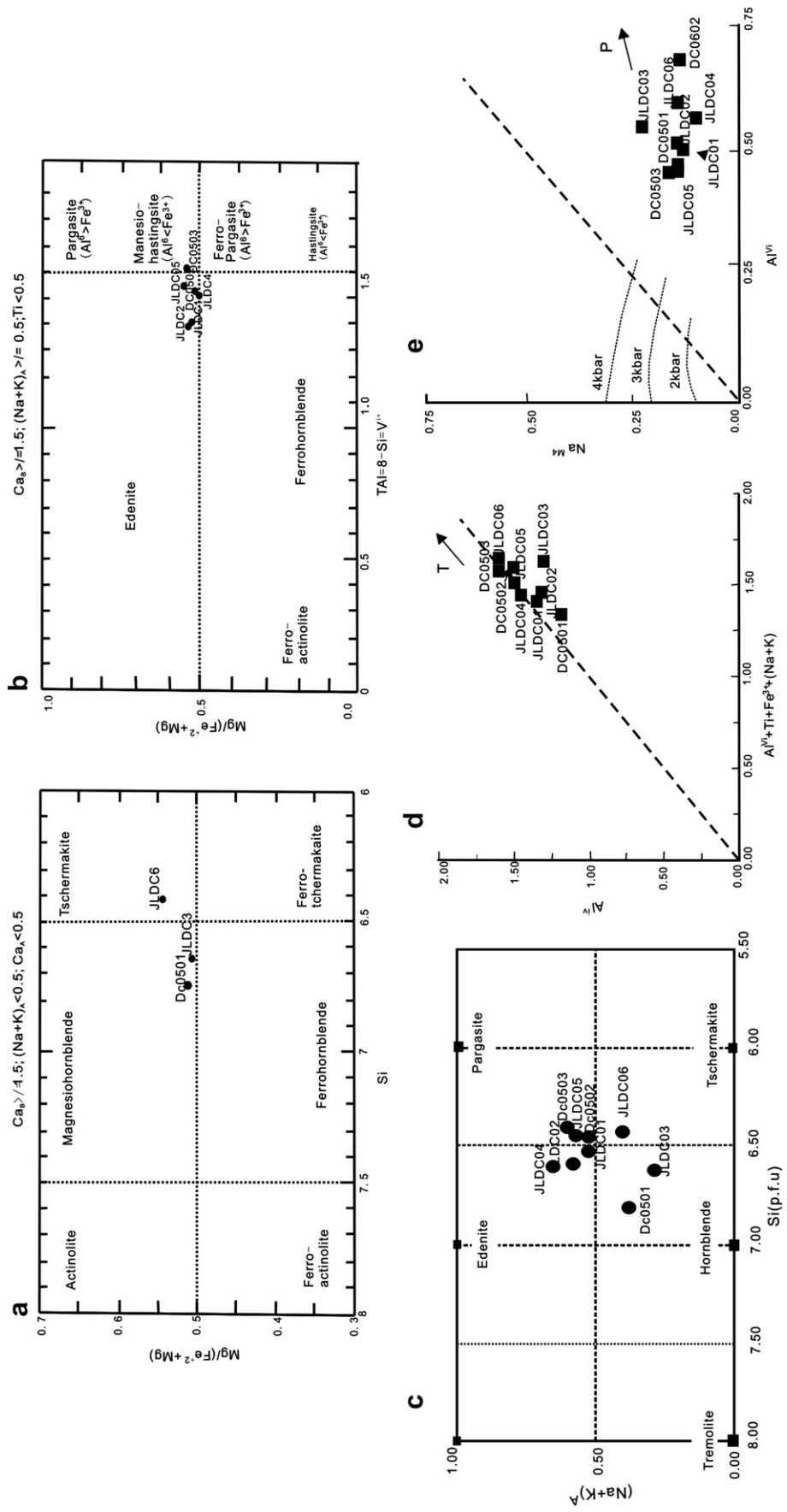

Fig. 10. Mineral chemistry of amphibole grains in the amphibolite mylonites. a. Si vs. Mg# diagram ($(Na + K)^A<0.5$); b. Al vs Mg# diagram ($(Na + K)^A>/ = 0.5$). Classification according to Leake et al. (1997); c. $(Na + K)^A$ vs. Si (p.f.u.) classification of calcic amphiboles according to Pe-Piper (1988). d. Al^{iv} vs. $Al^{vi} + Ti + Fe^{3+} + (Na + K)^A$ plot by Robison et al. (1971) is depicted by a 1:1 line that intersects at (0, 0); Increasing values along this line broadly indicates increasing temperature. e. Na^{M4} vs. Al^{vi} plot is indicated by a 1:1 line that intersects at (0, 0); increasing values along this line approximates a pressure increase; the isobarometric lines are deduced from the calibration by Brown (1977).

amphibole grains to the stretching lineation and foliation of the mylonites (Fig. 7c and d) implies that the lattice preferred orientation of dynamically recrystallized amphibole grains resulted from a dominant activation of (100) [001] slip (twinning) system.

Most fine grains in the matrix have close relationships with the type II porphyroclasts. During the deformation and recrystallization, the type II porphyroclasts have initial crystallographic orientations that are propitious for the (100) [001] slip system to be activated and therefore (100) micro-twinning becomes the most dominant deformation mechanism. Twinning is assisted by dislocation mobility, inducing well-organized dislocations along twin boundaries. Dominant (100) twinning is also proven by micro- and submicrostructural analysis. The existence of twin boundaries constrains the mobility of dislocations in twins and their hosts. TEM observation reveals the existence of two groups of dislocation walls in the type II porphyroclasts, one along (100) that constitute most of the twin boundaries, the other along (001) that form dislocation walls or subgrain boundaries in another direction (Fig. 5c). The curving directions of dislocation dipoles observed in the deformation twins suggest that dislocations glide or climb towards dislocation walls in the [001] slip direction.

(100) Twinning has accommodated the major strain that amphibole grains experienced. The most important role of twinning is that it contributes not only to deformation, but also to subgrain nucleation and subsequent dynamic recrystallization during shearing. Twins and their hosts are separated primarily by twin boundaries constituted by dislocations in (100) directions. In the twinned parts, dislocations glide or climb towards (100) twin boundaries or to (001) dislocation walls. The former enhances twin gliding, and the latter forms new boundaries that are subnormal to twin boundaries. Acicular to columnar-shaped subgrains are formed by combination of these twin boundaries along (100) and the (001) dislocation walls. Subsequent rotation of the subgrains is enhanced by progressive shearing and thus recrystallized new grains are formed. Both twins and their hosts evolve into fine grains that are parallel to each other. During this process, nucleation of the subgrains and subsequent formation of dynamically recrystallized fine grains are governed by both (100) twining and dislocation creep. We call this mechanism *twinning nucleation recrystallization (TNR)*(Fig. 11).

Fine grains formed by combined twinning and dislocation gliding/climbing are acicular to columnar in shape. They are homogeneously distributed in mylonitic matrix (more than 95% of the grains) and are aligned parallel to the shearing direction. It is optically very obvious that the generation of the fine grains in the matrix is related to the development of tails of type II mantled porphyroclasts; φ, σ or δ porphyroclasts. Some of the fine grains are further deformed during progressive shearing so that weak intragranular plastic deformation occurs in the grains.

In the amphibole mylonitic rocks, subgrain rotation due to dislocation glide and climb has partly contributed to the dynamic recrystallization processes. Dislocation walls, subgrains and dynamically recrystallized grains due to subgrain rotation are observed with TEM. Fine grains formed by subgrain rotation recrystallization are characterized by equigranular shapes. No or rare free dislocations are observed in the grains. OM observation reveals that the fine grains formed by subgrain rotation are much fewer than those formed by combined twining and dislocation creep.

7.3. Role of secondary phases: quartz and plagioclase

There is 30–35% plagioclase and 10–15% quartz in the amphibolite mylonitic rocks. They constitute quartzofeldspathic bands both in banded mylonites and in ultramylonites. Plagioclase grains in the mylonitic rocks are characterized by crystal plastic deformation and dynamic recrystallization. They are elongated or partly twinned, and some are dynamically recrystallized into fine

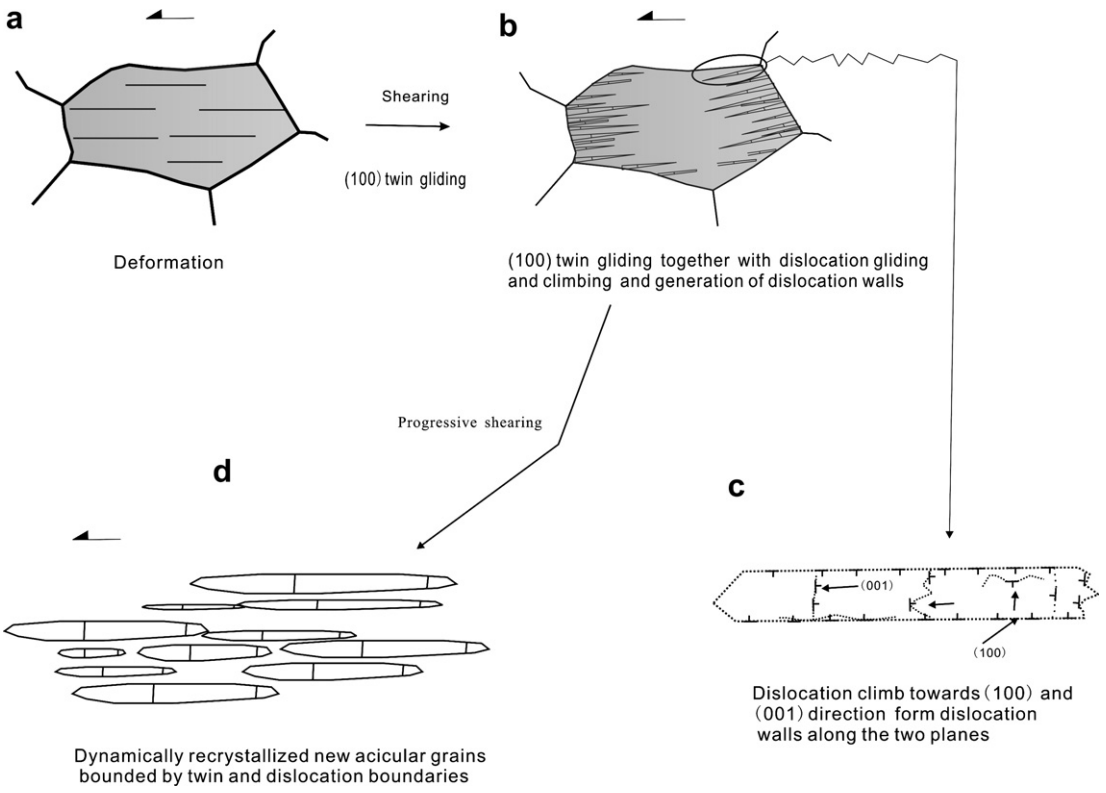

Fig. 11. Schematic diagram showing the dynamic recrystallization of amphibole by twinning nucleation recrystallization.

grains in the matrix. Undulatory and inhomogeneous extinction, grain elongation, deformation twinning and subgrain formation are common in porphyroclastic plagioclase grains. Quartz grains may form monomineralic bands or constitute polymineralic bands with plagioclase grains. They are characterized by high temperature grain growth, forming equant grains with straight boundaries and triple junctions (Fig. 3e and f), or rectangular quartz ribbons parallel to the dominant foliation in the mylonites. The latter often occur in high temperature tectonites (e.g. Culshaw and Fyson, 1984; Hippertt et al., 2001). At the same time, the quartz grains do not show any evidence of intragranular plastic deformation, suggesting a quasi-static grain growth.

The following indications suggest that the quartzofeldspathic bands are the high strain zones in the banded mylonitic rocks. (1) Most plagioclase grains are dynamically recrystallized into very fine grains of less than 10 microns in sizes. Some relic porphyroclastic grains are observed and have high aspect ratios. They are intensively twinned and show abundant evidences for crystal plastic deformation. (2) Quartz grains occur as ribbon quartz (rectangular quartz grain aggregates) or augen-shaped grain aggregates, indicating intensive high temperature deformation. (3) Amphibole grains in the quartzofeldspathic bands are generally new fine grains formed by dynamic recrystallization. Their grain sizes are very small (less than 15 μm) in comparison with amphibole grains in the amphibole-rich bands (greater than 100 μm). (4) Amphibole grains in the quartzofeldspathic bands are homogeneously distributed and strongly oriented, parallel to the macroscopic stretching lineation.

TEM observation is in agreement with high temperature deformation and recrystallization of quartz and plagioclase in high strain zones. Most quartz grains have polygonal shapes and sharp and straight grain boundaries. They are generally dislocation free or in some cases contain a few free dislocations, which are attributed to progressive deformation (Fig. 6a and b). In contrast, plagioclase grains contain many dislocation substructures that support crystal plastic deformation and dynamic recovery/recrystallization. In cores of plagioclase porphyroclasts there are rarely tangled dislocations (Fig. 6c). Dislocations are organized into arrays or walls, and the latter form subgrain boundaries. New fine grains of plagioclase with few free dislocations are formed by subgrain rotation (Fig. 6d). The new fine grains have typical characteristics of dynamically recrystallized fine grains.

Optical and TEM observations suggest that during deformation and dynamic recrystallization of amphibole grains in the mylonitic rocks high temperature ductile flow dominate the deformation of quartz and plagioclase grains. The existence of quartzofeldspathic components leads to strain localization and strain softening during mylonitization, which is possibly an important triggering for the deformation and dynamic recrystallization of amphibole grains.

8. Conclusions

1) Various microstructures and sub-microstructures are developed in the amphibole mylonitic rocks from Diancang Shan. Different mineral phases in the rocks show distinct deformation characteristics. Amphibole and plagioclase grains are intensively deformed with obvious grain size reduction, but quartz grains are recrystallized dominantly by grain growth. Our observations suggest that amphibole grains from the mylonitic rocks are strongly deformed and dynamically recrystallized under low-pressure metamorphic conditions at temperature of 585–673 °C, with an average of 625 °C.
2) Two types of porphyroclasts, i.e. type I “hard” porphyroclasts and type II “soft” porphyroclasts can be observed in the mylonites. Type I “hard” porphyroclasts have their crystallographic orientation with [001]-axes normal or subnormal to the stretching lineation of the rocks. Type II porphyroclasts have their orientation with [001]-axes parallel or sub-parallel to the stretching lineation. The latter are easily deformed and recrystallized due to the crystallographic orientation which makes it easy to activate the (100) [001] slip system. The two types of porphyroclasts possess a diversity of micro- and sub-microstructures that characterize their “hard” and “soft” behaviors during mylonitization. A close genetic relation of the fine grains to the type II “soft” porphyroclasts is proven by SPO, LPO and misorientation analysis.
3) Twinning nucleation recrystallization (TNR) is one of the most important processes that operate during dynamic recrystallization of amphibole. TEM and EBSD analysis reveals the dominant roles of (100) twinning during deformation and grain size reduction of amphiboles. Twinning along (100), in combination with dislocation creep (gliding and climbing) governs the nucleation of subgrains and subsequent formation of dynamically recrystallized new fine grains.

Acknowledgements

This study has received financial support from the National Natural Science Foundation of China (90814006, 40872139 and 40772133), the 111 Project (B07011) of the Ministry of Education and State Key Laboratory of Geological Processes and Mineral Resources (Grant No. GPMR200837). The authors acknowledge Prof. JIN Zhenmin and Dr. XU Haijun from China University of Geosciences at Wuhan for helpful discussions on apart of EBSD data analysis and Prof. Chunming Wu and Prof. Chunjing Wei for kindly help with the amphibolite geothermobarometri data analysis. The manuscript benefited immensely from the constructive reviews of one anonymous reviewer and Manuel Díaz Azpiroz as well as the journal editor Prof. Tom Blenkinsop.

References

Allison, I., La Tour, T.E., 1977. Brittle deformation of amphibole in a mylonite: a direct geometrical analogue of ductile deformation by translation gliding. Journal of Asian Earth Sciences 14, 1953–1958.
Anderson, J.L., Smith, D.R., 1995. The effects of temperature and f02 on the AL-in amphibole barometer. American Mineralogist 80, 549–559.
Babai, H.A., La Tour, T.E., 1994. Semibrittle and cataclastic deformation of amphibole-quartz rocks in a ductile shear zone. Tectonophysics 229, 19–30.
Barruol, G., Kern, H., 1996. Seismic anisotropy and shear-wave splitting in lower-crustal and upper-mental rocks from the Ivrea Zone-experimental and calculated data. Physics of the Earth and Planetary Interiors 95, 175–194.
Berger, A., Stünitz, H., 1996. Deformation mechanisms and reaction of amphibole: examples from the Bergell tonalite (Central Alps). Tectonophysics 257, 149–174.
Biermann, C., 1981. (100) Deformation twins in naturally deformed amphiboles. Nature 292, 821–823.
Biermann, C., Van Roermund, K.L.M., 1983. Defect structures in naturally deformed clinoamphiboles -a TEM study. Tectonophysics 95, 267–278.
Blundy, J.D., Holland, T.J.B., 1990. Calcic amphibole equilibria and a new amphibole-plagioclase geothermometer. Contributions to Mineralogy and Petrology 104, 208–224.
Brenker, F.E., Prior, D.J., Müller, W.F., 2002. Cation ordering in omphacite and effect on deformation mechanism and lattice preferred orientation (LPO). Journal of Structural Geology 24, 1991–2005.
Brodie, K.H., Rutter, E., 1985. On the relationship between deformation and metamorphism with special reference to the behavior of basic rocks. In: Thompson, A.B., Rubie, D.C. (Eds.), Metamorphic Reactions: Kinetics, Textures, and Deformation. Advances in Physical Geochemistry, vol. 4. Springer, Berlin, pp. 138–179.
Brown, E.H., 1977. The crossite content of Ca-amphibole as a guide to pressure of metamorphism. Journal of Petrology 18, 53–72.
Buck, P., 1970. Verformung von Amphibole-Einkristallen bei drucken bis 21 kb. Contributions to Mineralogy and Petrology 28, 62–71.
Burchfiel, B.C., Wang, E., 2003. Northwest-trending, middle Cenozoic, left-lateral faults in southern Yunnan, China, and their tectonic significance. Journal of Structural Geology 25, 781–792.
Burg, J.P., Wilson, C.J.L., Mitchell, J.C., 1986. Dynamic recrystallization and fabric development during the simple shear deformation of ice. Journal of Structural Geology 8, 857–870.

Culshaw, N., Fyson, W., 1984. Quartz ribbons in high grade gneiss: modifications of dynamically formed orientations by oriented grain growth. Journal of Structural Geology 6, 663–668.
Cumbest, R.J., Drury, M.R., Van Roermund, H.L.M., Simpson, C., 1989. Dynamic recrystallization and chemical evolution of clinoamphibole from Senja Norway. Contributions to Mineralogy and Petrology 101, 339–349.
De Meer, S., Drury, M.R., De Bresser, J.H.P., Pennock, G.M. (Eds.), 2002. Deformation Mechanisms, Rheology and Tectonics: Current Issues and New Developments in Deformation Mechanisms, Rheology and Tectonics. Geological Society, London, Special Publications, 200.
Díaz Azpiroz, M., Lloyd, G.E., Fernández, C., 2007. Development of lattice preferred orientation in clinoamphiboles deformed under low-pressure metamorphic conditions. A SEM/EBSD study of metabasites from the Aracena metamorphic belt (SW Spain). Journal of Structural Geology 29, 629–645.
Díaz Aspiroz, M., Fernández, C., 2003. Characterization of tectono-metamorphic events using crystal size distribution (CSD) diagrams. A case study from the Acebuches metabasites (SW Spain). Journal of Structural Geology 25, 935–947.
Dollinger, G., Blacic, J.D., 1975. Deformation mechanisms experimentally and naturally deformed amphiboles. Earth Planetary Science Letters 26, 409–416.
Drury, M.R., Ural, J., 1990. Deformation-related recrystallization processes. Tectonophysics 172, 235–253.
Ernst, W.G., Liu, J., 1998. Experimental phase-equilibrium study of Al- and Ti-contents of calcic amphibole in MORB-A semiquantitative thermobarometer. American Mineralogist 83, 952–969.
Fliervoet, T.F., Drury, M.R., Chopra, P.N., 1999. Crystallographic preferred orientations and misorientations in some olivine rocks deformed by diffusion or dislocation creep. Tectonophysics 303, 1–27.
Hacker, B.R., Christie, J.M., 1990. Brittle/ductile and plastic/cataclastic transition in experimentally deformed and metamorphosed amphibolite. In: Duba, A.G., Durham, W.B., Handin, J.W., Wang, H.F. (Eds.), The Brittle–Ductile Transition in Rocks. AGU Geophysical Monograph Series 56, pp. 127–148.
Hippertt, J., Rocha, A., Lana, C., Egydio-Silva, M., Takeshita, T., 2001. Quartz plastic segregation and ribbon development in high-grade striped gneisses. Journal of Structural Geology 23, 67–80.
Holland, T.J.B., Blundy, J.D., 1994. Non-ideal interactions in calcic amphiboles and their bearing on amphibole-plagioclase thermometry. Contributions to Mineralogy and Petrology 116, 433–447.
Imon, R., Okudaira, T., Fujimoto, A., 2002. Dissolution and precipitation processes in deformed amphibolites: an example from the ductile shear zone of the Ryoke metamorphic belt, SW Japan. Journal of Metamorphic Geology 20, 297–308.
Imon, R., Okudaira, T., Kanagawa, K., 2004. Development of shape- and lattice-preferred orientations of amphibole grains during initial cataclastic deformation and subsequent deformation by dissolution–precipitation creep in amphibolites from the Ryoke metamorphic belt, SW Japan. Journal of Structural Geology 26, 793–805.
Jiang, Z., Skrotzki, W., 1996. Microstructure and texture of amphibole from an amphibolite of the KTB main borehole (NE-Bavaria). Zeitschrift für Geologische Wissenschaften 24, 657–669.
Kenkmann, T., 2000. Processes controlling the shrinkage of porphyroclasts in gabbroic shear zones. Journal of Structural Geology 22, 471–487.
Kitamura, K., 2006. Constraint of lattice-preferred orientation (LPO) on Vp anisotropy of amphibole-rich rocks. Geophysical Journal International 165, 1058–1065.
Kruse, R., Stünitz, H., 1999. Deformation mechanisms and phase distribution in mafic high-temperature mylonites from the Jotun Nappe, southern Norway. Tectonophysics 303, 223–249.
Lacassin, R., Leloup, P.H., Tapponnier, P., 1993. Bounds on strain in large Tertiary shear zones of SE Asia from boudinage restoration. Journal of Structural Geology 15, 677–692.
Lafrance, B., Vernon, R.H., 1993. Mass transfer and microfracturing in gabbroic mylonites of the Guadalupe igneous complex, California. In: Boland, J.N., Fitz Gerald, J.D. (Eds.), Defects and Processes in the Solid State: Geoscience Applications, the McLaren Volume. Developments in Petrology, vol. 4, pp. 151–167.
Lapworth, T., Wheeler, J., Prior, D., 2002. The deformation of plagioclase investigated using electron backscatter diffraction crystallographic preferred orientation data. Journal of Structural Geology 24, 387–399.
Leake, B.E., Wolley, A.R., Arps, C.E.S., et al., 1997. Nomenclature of amphiboles. Report of the Subcommittee on amphiboles of International Mineralogical Association, Commission on New minerals and mineral Names. American Mineralogist 82, 1019–1037.
Lee, K.L., Jiang, Z., Karato, S., 2002. A scanning electron microscope study of the effects of dynamic recrystallization on lattice preferred orientation in olivine. Tectonophysics 351, 331–341.
Leiss, B., Gröger, H.R., Ullemeyer, K., Lebit, H., 2002. Textures and microstructures of naturally deformed amphibolites from the northern Cascades, NW USA: methodology and regional aspects. In: De Meer, S., Drury, M.R., De Bresser, J.H.P., Pennock, G.M. (Eds.), Deformation Mechanisms, Rheology and Tectonics: Current Status and Future Perspectives. Geological Society, London, Specical Publications 200, pp. 219–238.
Leloup, P.H., Harrison, T.M., Ryerson, F.J., Ryerson, F.J., Chen, W.J., Li, Q., Tapponnier, P., Lacassin, R., 1993. Structural, petrological and thermal evolution of a Tertiary ductile strike-slip shear zone, Diancang Shan, Yunnan. Journal of Geophysical Research 98, 6715–6743.
Leloup, P.H., Arnaud, N., Lacassin, R., Kienast, J.R., Harrison, T.M., Pan Trong, T.T., Replumaz, A., Tapponnier, P., 2001. New constraints on the structure, thermochronology and timing of the Ailao Shan–Red River shear zone, SE Asia. Journal of Geophysical Research 106, 6683–6732.
Leloup, P.H., Lacassin, R., Tapponnier, P., Schärer, Urs, Zhong, D.l., Liu, X.H., Zhang, L.S., Ji, S.C., Trinh, P.T., 1995. The Ailao Shan-Red River shear zone (Yunnan, China), Tertiary transform boundary of Indochina. Tectonophysics 251, 3–84.
Liu, J.L., Cao, S.Y., Zhai, Y.F., Song, Z.J., Wang, A.J., Xiu, Q.Y., Cao, D.H., Gao, L., Guan, Y., 2007. Rotation of crustal blochs as an explanation of Oligo-Miocene extension in Southeastern Tibet-evidenced by the Diancang Shan and nearby metamorphic core complexes. Earth Science Frontiers 14, 40–48.
Liu, J.L., Song, Z.J., Cao, S.Y., Zhai, Y.F., Wang, A.J., Gao, L., Xiu, Q.Y., Cao, D.H., 2006. The dynamic setting and processes of tectonic and magmatic evolution of the oblique collision zone between Indian and Eurasian plates: exemplified by the tectonic evolution of the Three River region, eastern Tibet (in Chinese). Acta Petrologica Sinica 22, 775–786.
Liu, J.L., Wang, A.J., Cao, S.Y., Zou, Y.X., Tang, Y., Chen, Y., 2008. Geochronology and tectonic implication of migmatites from Diancangshan, Western Yunnan, China. Acta Petrologica Sinica 24 (3), 413–420.
Liu, Y.C., 1999. Crystallographic preferred orientation and slip system of amphibole in the Florence shear zone, Central Australia. Journal of Mineralogy and Petrology 19, 1–7.
Lloyd, G.E., Farmer, A.B., Mainprice, D., 1997. Misorientation analysis and the formation of subgrain and grain boundaries. Tectonophysics 279, 55–78.
Mainprice, D., Nicolas, A., 1989. Development of shape and lattice preferred orientations: application to the seismic anisotropy of the lower crust. Journal of Structural Geology 11, 175–189.
Morley, C.K., 2007. Variations in Late Cenozoic–Recent strike-slip and oblique-extensional geometries, within Indochina: the influence of pre-existing fabrics. Journal of Structural Geology 29, 36–58.
Morrison-Smith, D.J., 1976. Transmission electron microscopy of experimentally deformed hornblende. American Mineralogist 61, 272–280.
Nyman, M.W., Law, R.D.S., Melik, E.A., 1992. Cataclastic deformation for the development of core mantle structures in amphibole. Geology 20, 455–458.
Passchier, C.W., Trouw, R.A.J., 2005. Microtectonics. Springer-Verlag, Berlin.
Pe-Piper, G., 1988. Calcic amphiboles of mafic rocks of the Jeffers Brook plutonic complex, Nova Scotia, Canada. American Mineralogist 73, 993–1006.
Randle, V., 1993. The Measurement of Grain Boundary Geometry. Institute of Physics Publishing, Bristol, 169 pp.
Robison, P., Ross, M., Jaffe, H.W., 1971. Composition of the anthophylite-gedrite series, comparisons of gedrite and amphibole, and the anthophyllite-gedrite solvus. American Mineralogist 56, 1005–1041.
Rooney, T.P., Riecker, R.E., Ross, M., 1970. Deformation twins in amphibole. Science 169, 173–175.
Rooney, T.P., Riecker, R.E., Gavasci, A.T., 1975. Amphibole deformation features. Geology 3, 364–366.
Schärer, U., Zhang, L.S., Tapponnier, P., 1994. Duration of strike-slip movements in large shear zones: the Red River belt. Earth and Planetary Science Letters 126, 379–397.
Sha, S.L., 1998. The basic features of Diancang Shan M T metamorphic zone (in Chinese). Yunnan Geology 1, 1–16.
Sha, S.L., Yin, G.H., Ao, D., Duan, G.X., 2002. Discovery and significance of ophiolitic mélanges at Diancang Shan Mountain in northwestern Yunnan. Regional Geology of China 29, 44–47.
Shelley, D., 1994. Spider texture and amphibole preferred orientations. Journal of Structural Geology 16, 709–717.
Skrotzki, W., 1992. Defect structures and deformation mechanisms in naturally deformed amphibole. Physics Status Solid 131, 605–624.
Spear, F.S., 1981. An experimental study of amphibole stability and compositional variability amphibolite. American Journal of Science 281, 697–734.
Spear, F.S., 1993. Metamorphic Phase Equilibria and Pressure-Temperature-Time Paths. Mineralogical Society of America, Washington, D.C.
Stünitz, H., 1993. Transition from fracturing to viscous flow in a naturally deformed metagabbro. In: Boland, J.N., Fitz Gerald, J.D. (Eds.), Defects and Processes in the Solid State: Geoscience Applications, the McLaren Volume. Developments in Petrology, vol. 4, pp. 121–150.
Tatham, D.J., Lloyd, G.E., Butler, R.W.H., 2008. Amphibole and lower crustal seismic properties. Earth and Planetary Science Letters 267, 118–128.
Trimby, P.W., Prior, D.J., Wheeler, J., 1998. Grain boundary hierarchy development in quartz mylonite. Journal of Structural Geology 20, 917–933.
Zhong, D.L., Tapponnier, P., Wu, H.W., 1990. Large-scale strike-slip fault, the major structure of intracontinental deformation after collision. Chinese Science Bulletin 35, 304–309.